2018

Investigating the Tumor Suppressor Role of RUNX1 in Human Breast Cancer

Adam S. Weinheimer
The University of Vermont

Investigating the Tumor Suppressor Role of RUNX1 in Human Breast Cancer

Adam Weinheimer[1]

May 2018

Thesis Committee Chair: Jay Silveira[2]
Thesis Advisors: Janet Stein[2] & Matthew Liptak[3]
Committee Member: Sayyed Kaleem Zaidi[2]
Research Mentor: Andrew Fritz[2]

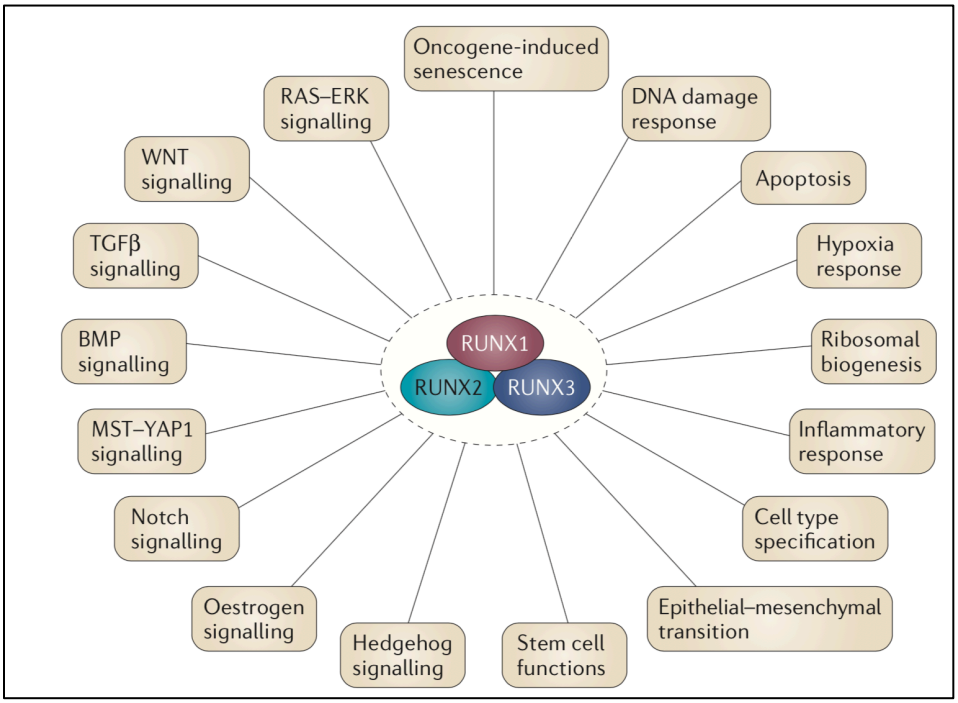

Ito Y, Bae SC, Chuang LS. The RUNX family: developmental regulators in cancer. Nat Rev Cancer (2015).

[1]The University of Vermont, Department of Biochemistry, College of Arts & Sciences
[2]The University of Vermont, Department of Biochemistry, Larner College of Medicine
[3]The University of Vermont, Department of Chemistry, College of Arts & Sciences

Abstract

Breast cancer (BrCa) remains the leading cause of cancer-related deaths in women worldwide (2). Current research suggests that the transcription factor RUNX1 functions as a regulator and potentially as a tumor suppressor in breast cancer progression (4). RUNX1 is the most dominant RUNX family member expressed in normal mammary epithelial cells (10) and it has been demonstrated that RUNX1 activity decreases as breast cancer aggression increases. Yet, the mechanism of this regulation remains unclear. The significance of this project is to further the in-depth investigation of the relationship between RUNX1 and differentially expressed genes that influence human breast cancer progression. This study addresses the hypothesis that RUNX1 controls a myriad of genes that play roles in the suppression of the breast cancer stem cell (BCSC) population, a subpopulation of cancer cells that are capable of self-renewal and demonstrate an ability to resist common chemotherapies and treatments. BCSCs are therefore the most dangerous and most essential to eradicate if the cancer is to be cured (11). To test this hypothesis, RUNX1 was downregulated in the MCF10A breast cancer cell line using both the inducible CRISPRi and the shRNA-mediated gene knockdown approaches. Fluorescence-activated cell sorting (FACS) and quantitative polymerase chain reaction (qPCR) confirmed successful knockdown of RUNX1 and further genetic and proteomic expression analyses of known breast cancer driver genes was performed to determine how RUNX1 depletion exerts control over the progression of BrCa. It was found that RUNX1 may aid in maintaining the epithelial phenotype in BrCa while also suppressing the expression of key BrCa driver genes such as phosphatidylinositol-3-kinases (PI3K) PIK3CA and PIK3R1. Investigating the role of RUNX1 as a suppressor of the BCSC population adds a new level of knowledge to the

field of breast cancer research, and may allow development of a safer, more targeted, and more effective plan of action to eradicate one of the deadliest diseases that exists today.

Introduction

Cancer is an incredibly complex and diverse disease that has the potential to affect every cell, tissue and organ of the body. Cancers touch every area of the globe and do not distinguish among age, sex, race, or ethnicity. Yet, underlying all cancers are key cellular and molecular hallmarks that allow cancers to evolve into lethal neoplastic diseases we see every day, from acute myeloid leukemia to breast cancer.

For decades, the cellular and molecular foundation of cancer cells has been explained as six hallmarks that contribute to the canonical cancer cell: a cell that displays an ability to rapidly grow, proliferate and divide, eventually becoming immortal and capable of invasion and metastasis. By sustaining proliferative signaling via an array of tyrosine kinase domains, paracrine or autocrine signaling, the cancer cell exhibits chronic proliferation that is largely out of control (5). This fundamental property of the cancer cell is further compounded by its ability to evade the regulatory suppression of growth. Contact inhibition is abolished and a net loss of the canonical growth suppressors that include retinoblastoma-associated protein (RB1) and TP53, a well-documented protein with anticancer activity via DNA damage response and cell cycle control, is often seen. In parallel to the cancer cell evading suppression of growth, the ability to resist cell death is also a characteristic of cancers. In a healthy cell, hyperproliferation often leads to increased DNA damage, which is sensed by the cell to either fix the DNA damage or induce apoptosis if the damage is too severe to be repaired. As these DNA damage sensors are lost, the apoptotic cascade fails, allowing the DNA damaged cell to continue

hyperproliferation (5). As these events transpire, the cell may soon reach a state of immortalization, in which repetitive divisions and growth do not result in cell senescence or crisis.

In order for a cancer cell to sustain the proliferative state, nutrient and energy requirements must still be met. The cell requires oxygen, nutrients, and an outlet for waste products such as carbon dioxide. As the cancer cell continues to mutate and progress, the angiogenic switch, often seen in embryonic and prenatal development, is turned on via hypoxia and oncogene signaling (5). This supports neoplastic growth by continually sprouting new blood vessels for nutrient delivery and waste removal. In the most progressive state, the cancer will activate mechanisms that allow for invasion and metastasis. It is thought that the loss of cell to cell and cell to extracellular matrix adhesion molecules allows the cancer to spread throughout the body. It is at this stage where the epithelial to mesenchymal transition (EMT) has been observed, a regulatory pathway that allows the cell to invade, metastasize, and resist the normal apoptotic programs. Key transcriptional factors are at play during EMT, most notably Snail, Slug, Twist, and Zeb1/2, all of which function to cause a net loss in cellular E-cadherin, a key cellular adhesion molecule (12). This marks the process known as the invasion-metastasis cascade. Following local invasion, intravasation occurs allowing the cell to travel throughout the circulatory and lymphatic systems. The cell then leaves this mode of transit via extravasation to settle in a distant part of the body, ideally one that provides a rich microenvironment for the cell to colonize the area and eventually grow into a macroscopic tumor. Most often, this cascade results in the cancer cell colonizing a niche environment, an area of the body that is rich in nutrients necessary for cellular survival. As these events transpire in a successive

manner, the result is an invasive subpopulation of cancer that can be aggressive and often lethal.

In just the last decade, tumors have been categorized as functioning and complex organs. No longer can a tumor be simply considered a collection of homogenous cells. Rather, a tumor is made up of a diverse array of heterogeneous cells, each type specialized in its own way and harboring unique mutations (5). These types may include, but are not limited to, local stem and progenitor cells, immune inflammatory cells, cancer cells, pericytes, endothelial cells, cancer-associated fibroblasts, invasive cancer cells, and cancer stem cells (CSCs) (11). Each of these cell types performs a unique function within the tumor organ and the tumor microenvironment. Immune inflammatory cells, for example, demonstrate tumor-promoting as well as tumor-suppressive subtypes (Figure 1).

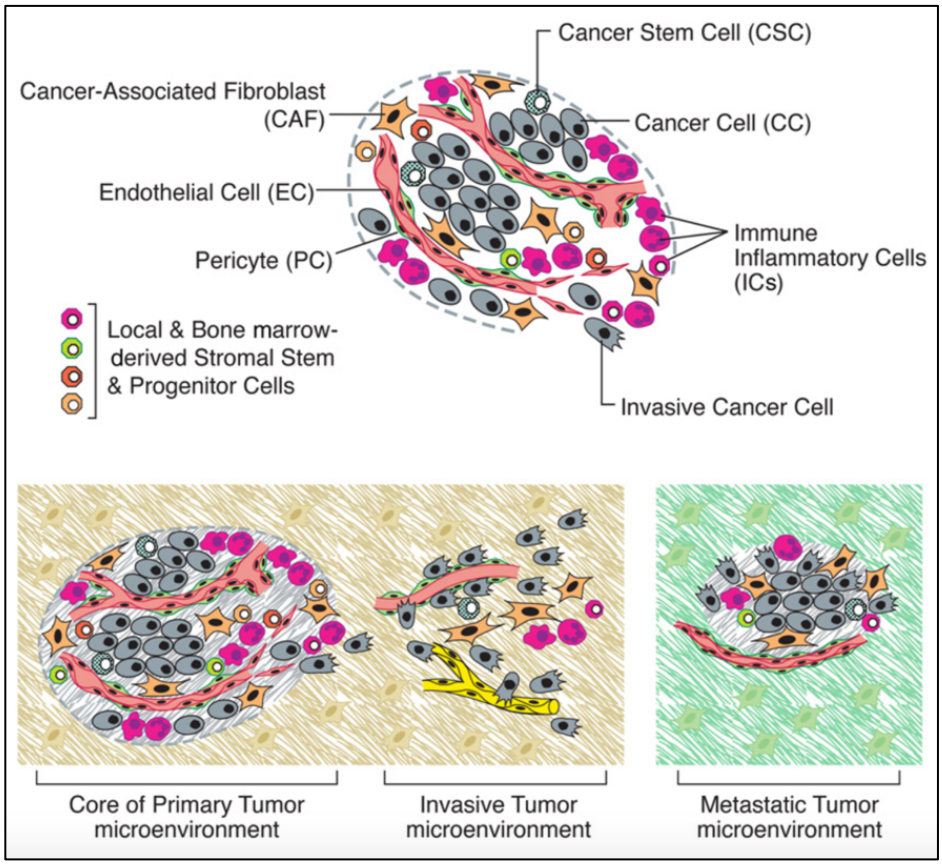

Acquired from Hanahan D, Weinberg RA. Hallmarks of cancer: the next generation. Cell. 2011

Figure 1: The Heterogenous Cells of the Tumor Microenvironment. A multitude of cell types constitute solid tumors that together enable tumor growth and progression (upper). The characteristics of the cells evolve as they progress from a primary tumor, to an invasive or metastatic state (lower) (5).

Recently, CSCs have come to the forefront of cancer research, as these cells are able to propagate new tumors upon host inoculation. Additionally, CSCs characteristically display expression of markers that are also found on stem cells in the same tissue-of-origin. Similar to healthy stem cells, CSCs are capable of self-renewal and therefore pose a significant threat when coupled with the canonical trademarks of a cancer cell (11). One such threat is an increased resistance to some of the most widely used cancer therapies today, such as chemotherapy. Furthermore, when a subpopulation of the tumor is resistant to chemotherapeutics, the treatment behaves as a selective pressure on the cancer population, allowing only the resistant CSCs to survive and foster a stronger and potentially deadly patient relapse. Investigating CSCs is therefore critical to understand how cancer progresses and to develop cancer therapies that truly eradicate the genetically heterogeneous tumor.

In mammals, three RUNX genes encode transcription factors that serve as master regulators of development. RUNX1, RUNX2, and RUNX3 each display unique expression patterns that are critical to certain tissues and organ systems (4). RUNX proteins operate as effectors of crucial developmental pathways, including transforming growth factor-β (TGF-β), WNT, Notch, and receptor tyrosine kinases (4). This has led the RUNX family to be an important area of interest in oncological and carcinogenesis research. RUNX1 is essential for normal hematopoiesis and is heavily involved in human leukemia, while RUNX2 is an important bone lineage factor involved in osteosarcoma. In metastatic breast and prostate cancers, RUNX2 is often overexpressed, pointing to a role in tumorigenesis and metastasis (4).

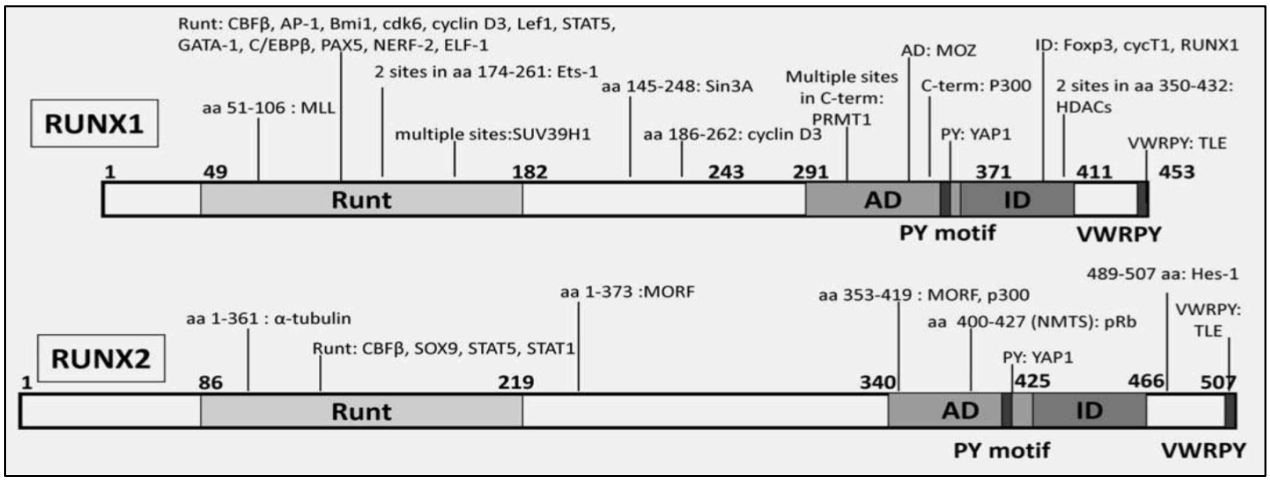

Figure 2: Functional domains of RUNX proteins and their interacting proteins. RUNX proteins contain a highly conserved Runt domain at the N-terminus at which CBF**β** and DNA bind. The Runt domains exhibit 90% homology among all RUNX family members (8).

The *RUNX1* gene is located on the long arm of chromosome 21 (21q22.12) and expression of RUNX1 is regulated by two promoters known as P1 (distal) and P2 (proximal) (8). Due to alternative splicing, the *RUNX1* gene is capable of producing several isoforms that encode proteins with unique properties. Each RUNX family member contains a highly conserved DNA-binding domain known as the Runt domain (Figure 2). It is in this domain that the heterodimeric binding partner, core-binding factor-beta (CBFβ), binds and displaces the inhibitory domain of RUNX. CBFβ is therefore crucial to gene regulation of the developmental pathways of hematopoiesis and osteogenesis (13). Though CBFβ does not directly bind DNA, it exerts control by allosterically enhancing DNA binding at certain enhancers and gene promoters (13). The Runt domain is also subject to frequent mutations which result in an overall loss in DNA-binding ability. Furthermore, the RUNX proteins are subject to post-translation modifications, allowing the transcription factors to fulfill their role as master regulators of development. These modifications include methylation, acetylation, phosphorylation and ubiquitylation, all of which facilitate the impressive list of activating and inhibitory

developmental control mechanisms exerted by RUNX1 (4). RUNX1 also associates with cyclin-dependent kinases (CDKs), and its phosphorylation status determines the stability of the protein and the control of the cell transition from G_1 to S phase and further proliferation (4).

Due to the master regulator role of RUNX1 in developmental control, genomic dysregulation can lead to the onset of many types of cancer, especially those derived from hematopoietic cells. Similarly, RUNX1 aberrations resulting from specific chromosomal translocations and gene fusions lead to the onset of specific leukemia subtypes, such as the development of acute lymphoblastic leukemia (ALL) following t(12;21) and the resulting TEL-AML1 fusion gene (4).

As stated, the role of RUNX1 in hematopoiesis is well-known, but its function in epithelial cells is much less understood. RUNX proteins recognize a core genomic sequence (4) and recruit mediators of signaling pathways, chromatin remodelers, and chromatin organizing proteins to regulatory regions of target genes. These genes in turn coordinate the control of proliferation, growth and differentiation (8, 14, 15). Several reports have demonstrated a lower expression of RUNX1 across BrCa progression (3, 16, 17); RUNX1 expression decreases as the aggression of the breast cancer increases (4). Therefore, in breast cancer specifically, increased RUNX1 expression is a characteristic of good prognosis, indicating that RUNX1 acts as a tumor suppressor (3). RUNX factors are implicated in normal mammary stem cell maintenance (18-21) and mammary gland development (22-25). Additionally, both RUNX1 and its heterodimeric binding partner CBFβ are prevalent among predicted driver mutations in BrCa (2, 26, 27). The majority of these mutations indicate a loss of function (28). Knockdown of RUNX1 facilitates estrogen-induced Wnt signaling (10), an epithelial to mesenchymal transition (3) and

morphological defects (29). Furthermore, RUNX1 contributes to p53-dependent DNA damage response, a key mechanism facilitated by the p53 tumor suppressor (3). There are conflicting reports whether RUNX1 acts as a tumor suppressor or an oncogene in BrCa; one explanation for this discrepancy may be due to the model that BrCa consists of a diverse group of subtypes (30). These BrCa subtypes have different cellular origins (luminal versus basal) and molecular alterations (e.g., hormonal status including ER, PR, and HER2) that result in malignancy. More work is required to determine the molecular mechanisms by which RUNX1 functions in BrCa.

Our research group has demonstrated that RUNX1 is involved in a key biological process, the epithelial to mesenchymal transition (EMT) (3). During EMT, epithelial cadherin (E-cadherin/CDH1) and tight cell-cell junctions are lost, allowing epithelial cells to transition to mesenchymal cells (31). Normally, EMT is a process crucial to development, most notably gastrulation and organ development during embryogenesis (12). However, EMT is also utilized by early stage tumors to form invasive malignancies in breast cancer (12). As a result of EMT, breast cancers display invasive properties that allow the cancer to metastasize and progress to a more aggressive state with a poorer prognosis. During progression, early stage cancer cells displaying the epithelial phenotype, a state that requires cell to cell contact and lacking mobility, transition to a mesenchymal phenotype. Mesenchymal cells lack a polarized cytoskeleton and therefore display a change in cellular morphology that is more spindle-shaped, aiding in the cell's ability to metastasize and survive with reduced cell to cell contact (Figure 3) (3).

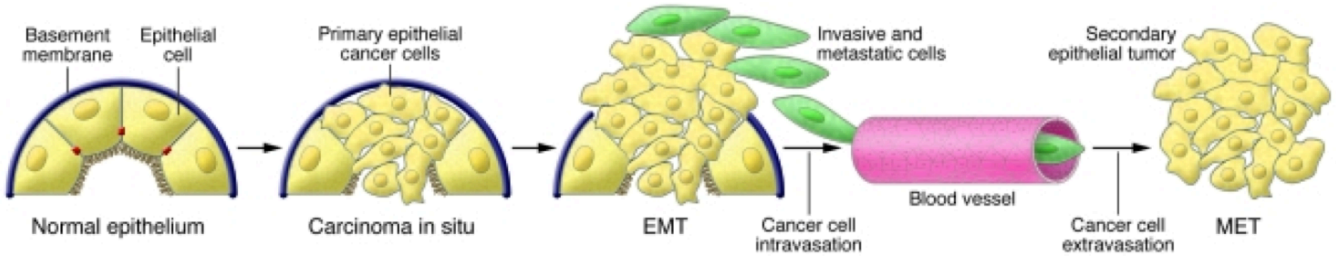

Figure 3: The Epithelial to Mesenchymal Transition contributes to the progression of cancer. As EMT progresses, cells lack cellular adhesion markers such as E-cadherin and express mesenchymal markers vimentin and N-cadherin. The mesenchymal phenotype contributes to cellular invasion and cancer metastasis (6).

Recent research demonstrates that RUNX1 maintains the normal epithelial phenotype and that RUNX1 expression is inversely related to the relative aggression of breast cancer (3). For instance, in the MCF10 breast cancer cell line progression series, RUNX1 RNA expression decreases as the cancer aggression progresses from normal-like MCF10A mammary epithelial cells through tumorigenic MCF10AT1 cells to the metastatic MCF10CA1a cells (Figure 4A) (3). Furthermore, by quantitatively analyzing expression of the cellular markers E-cadherin and vimentin through the MCF10 series, EMT has been shown to progress as RUNX1 expression decreases (Figure 4B). This is exemplified by a decrease of E-cadherin expression and an increase in expression of vimentin, an intermediate filament present in mesenchymal cells. This relationship between RUNX1 and EMT further supports the role of RUNX1 as a tumor suppressor in breast cancer.

Moreover, upon shRNA-mediated knockdown of RUNX1 in MCF10A cells, E-cadherin exhibits a significant decrease in mRNA expression while both vimentin and N-cadherin, a known protein marker for cancer metastasis, display a significant increase in mRNA expression (Figure 5) (3).

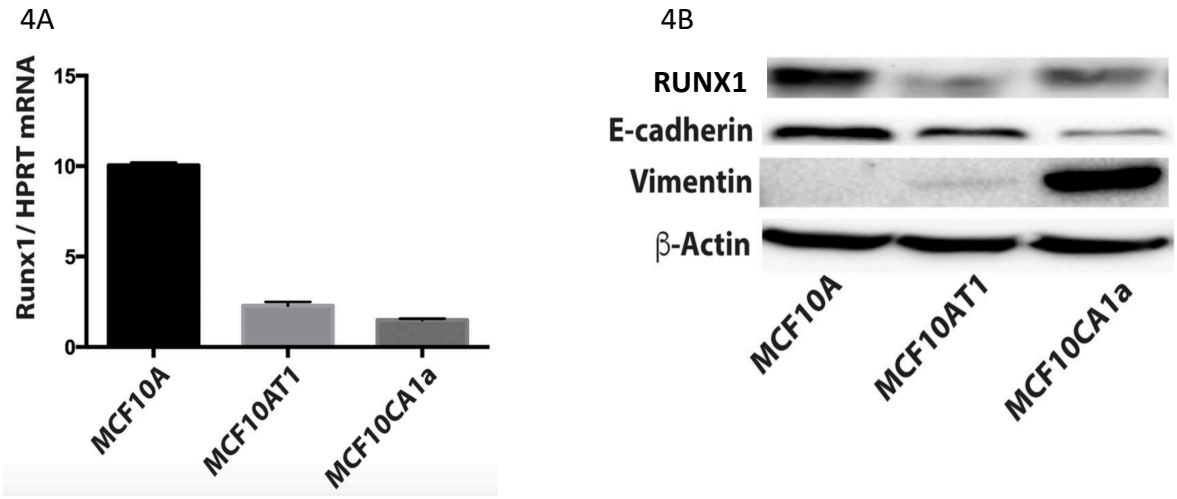

Figure 4: Expression profiles in the MCF10A Breast Cancer Cell Series. A: RUNX1 RNA expression by RT-qPCR of normal mammary-like MCF10A cells, MCF10A-derived tumorigenic MCF10AT1 cells, and metastatic MCF10CA1a cells demonstrates a reduction in RUNX1 as the series progresses. **B:** Protein expression by western blot analysis of the MCF10A series demonstrates a reduction in RUNX1 and E-cadherin and an increase in Vimentin as the series progresses to metastasis (3).

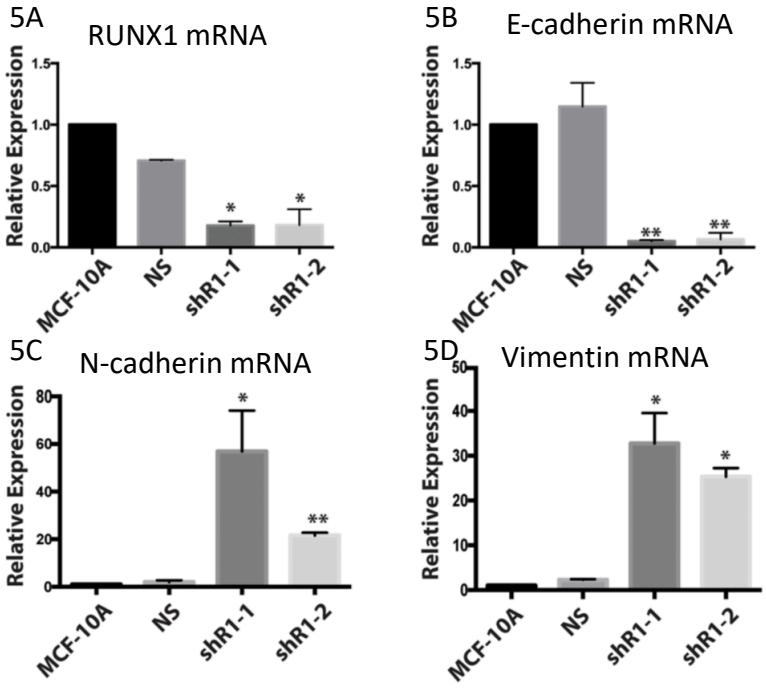

Figure 5: RUNX1 Depletion in MCF10A Cells Advances the Mesenchymal-like Phenotype. Western blot analyses of cell lysates show a decrease in RUNX1 expression (A) upon shRNA-mediated knockdown of RUNX1 relative to the non-silencing (NS) shRNA construct. A decrease in E-cadherin (B) is observed upon RUNX1 knockdown as well as an increase in the mesenchymal genes N-cadherin (C) and Vimentin (D) (3).

Recent studies have shown that overexpression of RUNX1 is able to rescue and reverse the EMT phenotype after TGFβ-induced EMT. Upon overexpression of RUNX1, E-cadherin mRNA expression increased while vimentin mRNA expression decreased. This rescue study therefore established the significant role of RUNX1 in preventing EMT (3). With the evidence of EMT progression as a result of RUNX1 knockdown, RUNX1 can be considered a tumor suppressor gene in mammary epithelial cells.

In all cancers, genomic mutations may be classified as driver or passenger mutations. A driver mutation is one that promotes the progression of the cancer and is causally implicated in doing so. Driver mutations confer growth advantages on the cancer and are therefore positively selected for in the tumor microenvironment. Conversely, mutations known as passenger mutations are not selected for, as they do not directly contribute to cancer development. Passenger mutations commonly occur during cellular division and do not carry severe functional consequences. Therefore, the more developed cancer will harbor a number of driver mutations along with a variety of passenger mutations that were carried throughout the development of the cancer (36). In 2016, Serena Nik-Zainal and colleagues analyzed whole genome sequences of 560 patient-derived breast cancers using massively-parallel sequencing to gain a better understanding of the genetic mutations driving BrCa, clonal advantages, and the processes generating these somatic mutations (1). Together with transcriptome sequencing, microRNA expression and DNA methylation data, as well as data from other studies (32-35), the authors analyzed information from a total of 1,332 breast cancers. Utilizing a list of 727 known human cancer genes (not specific to BrCa), this study found the 10 most frequently mutated genes in these 1,332 BrCa cases: *TP53, PIK3CA, MYC, CCND1, PTEN, ERBB2, GATA3,*

RB1, MAP3K1, and *chr8:ZNF703/FGFR1 (1).* These 10 common BrCa mutations accounted for 62% of the total 194 driver mutations found.

Modern day technologies that disrupt gene expression of a specific target serve as very powerful analytical tools in scientific research. One such tool developed in recent years is known as CRISPRi (clustered regularly interspaced short palindromic repeat interference). The system was discovered in bacteria, when three groups noticed that some CRISPR spacers were identical to sequences of viruses (37). A deeper look into the CRISPR array found that CRISPR-Cas (CRISPR associated proteins) systems are responsible for adaptive immunity in bacteria, with the ability to acquire fragments of foreign DNA and incorporate them into the genome to allow for sequence-specific resistance and degradation if that foreign DNA target were to invade the cell again (37). The CRISPR-Cas system has come to the forefront of research investigations interested in gene function, developmental pathways, and mechanisms of disease. In this project, inducible CRISPRi-dCas9-KRAB was utilized to specifically repress and knockdown the expression of RUNX1 in the MCF10A breast cancer cell series.

Another modern day technology critical to loss-of-function studies and gene depletion analyses is known as RNA interference (RNAi). The mechanism at work in RNAi is based on the sequence-specific degradation or translation interference of mRNA through the cytoplasmic delivery of double-stranded RNA that carries the identical sequence to the target gene (38). Target-specific degradation is achieved by use of the cell's endogenous RNA-induced silencing complex, commonly known as RISC, as well as the endogenous enzyme known as Dicer. Gene silencing is also achieved by siRNA binding the target mRNA to physically interfere with the

cell's translation machinery (39). In this project, shRNA was successfully utilized to knockdown the expression of RUNX1 in the MCF10 breast cancer cell series at the transcriptome level.

Future directions for this project include investigating the mechanism by which RUNX1 suppresses tumor progression. In response to RUNX1 knockdown, this project will analyze the downstream effects of genes known to be activated or suppressed as cancer progresses, commonly known as cancer driver genes. Through identification of potential BrCa driver genes regulated by RUNX1, further studies may investigate the role these genes have in the BCSC population; contributing important evidence for potential targets for modern, safe, and efficient BrCa therapies.

Methods

Tissue Culture

The MCF10A (10A) cell progression model was used for all experiments in this study. The MCF10 breast cancer cell progression series is derived from benign breast tissue from a woman with fibrocystic breasts. The MCF10A cells are immortalized, normal-like and non-malignant, attached epithelial cells, while the MCF10AT1 (AT1) cells are derived from MCF10A cells transformed with constitutively activated H-RAS, resulting in premalignant cells capable of neoplasm progression. The MCF10CA1a (CA1a) cells are the final cells in the progression, which are fully malignant, readily forming large tumors and capable of metastasizing. All three cell lines were produced from the same patient and thus have a similar genetic background.

The media used for both 10A and AT1 cells consisted of DMEM/F12 (Hyclone-SH30271.02) and 5% horse serum (Gibco 16050 lot #1075876) and 10ug/ml of human insulin (Sigma I-1882) and 20ng/ml of human epidermal growth factor and 100ng/ml of cholera toxin

(Sigma C-8052) and 0.5 ug/ml of Hydrocortisone (Sigma H-0888) and Pen/Strep, and L-Glutamine.

Cells were cultured in growth media, which was replaced every 24-48 hours by removing the old media and replacing with the new media warmed to 37°C. For a 100mm petri dish, 10mL of media was used. As the culture reached 75-80% confluency, the cells were passaged using a splitting ratio of approximately 1:10. The cells were passaged every 2-4 days as the cell density approached approximately 7-10 x 10^6 cells per 100mm dish. The seeding density for plating cells was approximately 1-2 x 10^6 cells per 100mm dish. All cell cultures were maintained at 37°C.

CRISPRi Oligo Design and Cloning

The CRISPRi-dCas9 system utilizes a doxycycline-inducible deactivated Cas9 protein fused to a KRAB (Krüppel-associated box) repression domain, targeting the RUNX1 gene and, upon addition of doxycycline, prevents transcription of nascent RUNX1 mRNA (40) (Figure 6). In the inducible CRISPRi system the target is not cleaved or excised, rather it is silenced and repressed when doxycycline is present. This is because the Cas9, which holds helicase and nuclease activity, has been deactivated (dCas9), resulting in a physical steric block that halts transcription elongation by RNA polymerase (41).

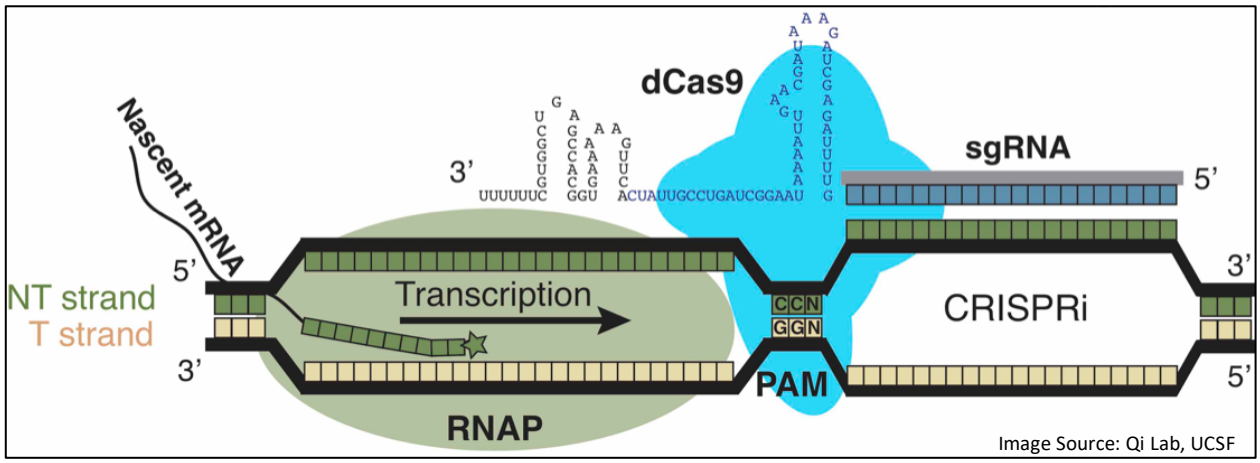

Figure 6: The Inducible CRISPRi-dCas9 System Halts Transcription Elongation by Interfering with RNA Polymerase. Upon dCas9 induction via doxycycline, dCas9 identifies a PAM sequence along with a gene target using a specific sgRNA sequence. Once bound, dCas9-KRAB block transcription of the target gene, generating a depletion of the target gene.

This differs from the original CRISPR system developed in 2012, which uses active RNA-guided nucleases to recognize, cleave and degrade any foreign genetic elements (40). The complete system is composed of CRISPRi dCas9-KRAB with a highly specific single guide RNA (sgRNA) for the target gene of interest. Additionally, the target locus must contain a specific protospacer adjacent motif (PAM) sequence, which in this case is NGG, where N is any nucleotide (40). The ability for inducible CRISPRi to be highly programmable for the target gene as well as completely reversible lends it to be one of the most useful tools in depletion and loss-of-function studies.

Guide RNAs were chosen to target between 300 base pairs upstream and 100 bases downstream of the RUNX1 transcription start site using the online tool Benchling CRISPR design. Three guides, each of 20 base pairs, were designed for each RUNX1 promoter of interest, denoted P1 and P2 (Table 1). All plasmids contained the same overhangs following digestion and were used for cloning into lentiCRISPRv2 (or lentiCRISPRv1). The overhangs were designed as shown below.

5’ – CACCGNNNNNNNNNNNNNNNNNN – 3’
3’ – CNNNNNNNNNNNNNNNNNNNCAAA – 5’

Construct #	Oligo 1	5' overhang	3'overhang	Oligo 2
1	CACCGTTTACTGTAAGCCCGGCCGG	AAAC	C	AAACCCGGCCGGGCTTACAGTAAAC
2	CACCGTCAGCTCGTTTGCATAGGGG	AAAC	C	AAACCCCCTATGCAAACGAGCTGAC
3	CACCGGGGCTGCGTACAGTAGCGCG	AAAC	C	AAACCGCGCTACTGTACGCAGCCCC
4	CACCGGCCGAGTAGACTTTGCAAGA	AAAC	C	AAACTCTTGCAAAGTCTACTCGGCC
5	CACCGAGTCACTTATTATATCTCAA	AAAC	C	AAACTTGAGATATAATAAGTGACTC
6	CACCGTGGCAAGAACCAATTGAGAT	AAAC	C	AAACATCTCAATTGGTTCTTGCCAC

Construct #	GeneID	Ensembl_ID	Guide #	Name		Sequence 20bp
1	P1	ENSG00000159216	955	P1955	CACCG	TTTACTGTAAGCCCGGCCGG
2	P1	ENSG00000159216	920	P1920	CACCG	TCAGCTCGTTTGCATAGGGG
3	P1	ENSG00000159216	815	P1815	CACCG	GGGCTGCGTACAGTAGCGCG
4	P2	ENSG00000159216	859	P2859	CACCG	GCCGAGTAGACTTTGCAAGA
5	P2	ENSG00000159216	813	P2813	CACCG	AGTCACTTATTATATCTCAA
6	P2	ENSG00000159216	990	P2990	CACCG	TGGCAAGAACCAATTGAGAT

Table 1: Design of Six CRISPRi Constructs Targeting Promoter 1 (P1) and Promoter 2 (P2) of hRUNX1. Benchling CRISPR Design was utilized to target the RUNX1 transcription start site and the automated DNA sequencing of the guides was performed in the University of Vermont Cancer Center Advanced Genome Technologies Core.

Standard de-salted oligos were ordered from Invitrogen and resuspended to 100μM in sterile water. Oligos were stored at -20°C. For each construct, each oligo pair was phosphorylated and annealed. 1μl of 100μM oligo 1 was combined with 1μl of 100μM oligo 2, 1μl 10X T4 Ligation Buffer, 0.5μl T4 PNK (NEB M0201S), and 6.5μl ddH_2O. The oligos were annealed in a thermocycler at 37°C for 30 minutes followed by 5 minutes at 95°C and subsequently ramped down to 25°C at 0.1°C/sec. The annealed oligos were pooled and diluted 1:250.

The digestion-ligation reaction was set-up by combining a variable volume of lentiguide-puro or other backbone vector (100ng), 2 μl of diluted phosphorylated and annealed oligo duplex, 2 μl 10x FastDigest Buffer, 1 μl 10mM DTT, 1 μl 10 mM ATP, 1 μl FastDigest Esp3I (Thermo Fisher), 0.5 μl T7 DNA ligase, and a variable volume of ddH_2O for a combined total of

20μl. A negative control digest using H_2O was also established for the reaction. The ligation reaction was incubated in a thermocycler for 5 minutes at 37°C followed by 5 minutes at 23°C, and these two steps were repeated through six total cycles and held at 4°C. The exonuclease treatment reaction consisted of 11μl of the ligation reaction, 1.5μl 10X PLasmidSafe Buffer, 1.5μl 10 mM ATP, and 1μl PlasmidSafe DNase and was incubated at 37°C for 30 minutes.

Plasmid (2μl) was transformed into 50μl of Stbl3 cells (Thermo Sci NC9046399) following mix-and-go protocol. The cell suspension (50μl) was plated on plates containing ampicillin. The following day, individual, homogenous bacteria cultures were selected using a sterile pipette.

shRNA-mediated Knockdown

Since the conception of early RNAi methods, such as small interfering RNA (siRNA), methods have evolved to use shRNA. shRNA constructs are capable of DNA integration and are therefore more stable and suitable for gene knockdown than siRNA (38). In shRNA, target constructs are infected into the cell using virally produced vectors or are transfected as plasmid vectors into the cell. The shRNAs consist of 19-22bp sequences linked by a short loop of nucleotides akin to that of the hairpin structure found in naturally occurring microRNA. After transcription of the newly integrated shRNA, the shRNA sequence is exported to the cytosol where it is bound by the Dicer enzyme. Dicer then processes the shRNA into siRNA duplexes 21-23 nucleotides long having 2-nucleotide-long 3'-overhangs on each strand, which subsequently bind the target mRNA for incorporation into the RISC complex or bind to physically prevent translation from occurring. RISC then unwinds the double-stranded siRNA and selects the antisense (guide) strand that is complementary to the knockdown target. Finally, RISC and the catalytically active subunit Argonaute protein family member (Ago) carry out the slicing function

by cleaving the RNA transcript that is paired to the guide strand. This cleaving action therefore prevents the expression of the gene product (Figure 7) (38, 42).

Recent studies achieving gene knockdown in mammalian cells have employed shRNA over siRNA for a few reasons (39, 43, 44). One major concern with siRNA is off-target effects due to the high concentration of siRNA in the cytoplasm. Though improved, this remains a concern for shRNA (38). Another major concern for siRNA is that as the cells divide, the siRNA concentration can become diluted, which can pose a significant issue with rapidly dividing cancer cells such as MCF10AT1. shRNA is preferred for this gene knockdown study because it can be used to create a stable cell-line via drug selection such as puromycin and fluorescent markers such as GFP that may be used for FACS (38).

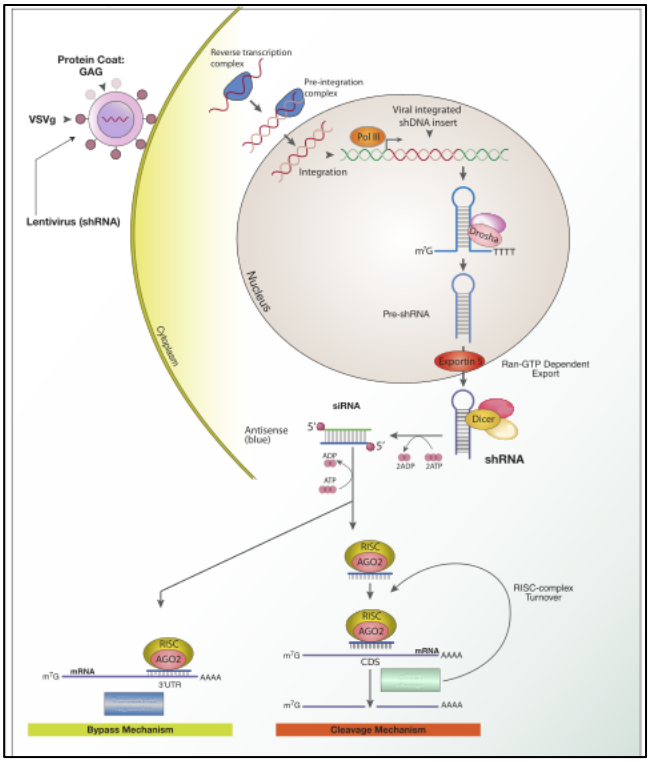

Figure 7: shRNA-Mediated Gene Silencing. The shRNA is exported to the cytosol where it is processed into siRNA duplexes that target the gene of interest for degradation via RISC (7).

Plasmid Isolation

Plasmid DNA was isolated using Zymo Research ZymoPURE Plasmid Midiprep Kit (D4200). This kit utilizes a modified alkaline lysis method of plasmid purification and ensures the plasmid is free of endotoxins, salts, proteins and RNA. Therefore, the prepared plasmids are suitable for transfection, transformation, PCR amplification and DNA sequencing. The kit was used according to manufacturer's instructions using the centrifugation method. The nucleic acid concentrations of each plasmid were analyzed using the ThermoFisher NanoDrop 2000 UV-Vis spectrophotometer.

Virus Production

HEK293T cells were maintained in Dulbecco's Modified Eagle Medium (Gibco, 11965) supplemented with 10% fetal bovine serum (Valley Biomedical, BS3033). HEK293T cells were split and plated at 1.3×10^5 cells/cm^2. The following day, packaging plasmids and dCas9 or sgRNA-coding plasmids were transfected using Lipofectamine 2000 transfection reagent (Invitrogen, 11668500) into HEK293T cells in Opti-MEM (Gibco, 31985) according to the manufacturer's instructions. Virus was harvested 48 hours after transfection. Plasmids containing either CRISPRi guide RNA or shRNA-RUNX1 were then transduced into 10A or AT1 cells. For inducible CRISPRi, dCas9 expression was induced by the addition of the antibiotic doxycycline. Fresh doxycycline was added to fresh media at the concentration of 2μM every 24 hours to maintain dCas9 expression and therefore maintain the inhibition of RUNX1 by CRISPR.

shRNA Knockdown: Infection

Lentivirus-based RNAi transfer plasmids with pGIPZ shRUNX1 (clone V2LHS_150257 and V3LHS_367631, GE Dharmacon) and pGIPZ non- silencing (Cat No. RHS4346, GE Dharmacon)

were purchased from Thermo Scientific. To generate lentivirus vectors, 293T cells in 10 cm culture dishes were co- transfected with 10 µg of pGIPZ shRUNX1 or pGIPZ non- silencing, with 5 µg of psPAX2, and 5 µg of pMD2.G using lipofectamine 2000 reagent (Life Technologies). Viruses were harvested every 48 h post-transfection. After filtration through a 0.45 µm-pore-size filter, viruses were concentrated by using LentiX concentrator (Clontech, Mountain View, CA, USA).

Gene delivery by transfection and infection

For shRNA-mediated knockdown of RUNX1 expression, MCF10A or MCF10AT1 cells were plated in six- well plates ($1x10^5$ cells per well) and infected 24 hours later with lentivirus expressing shRUNX1 or non-silencing (NS) shRNA. Briefly, cells were treated with 0.5 ml of lentivirus and 1.5 ml complete fresh DMEM-F12 per well with a final concentration of 4 µg/ml polybrene. Plates were centrifuged upon addition of the virus at 1460 × *g* at 37°C for 30 min. Infection efficiency was monitored by GFP co-expression at 2 days post infection. Cells were selected with 2 µg/ml puromycin (Sigma Aldrich P7255- 100MG) for at least two additional days. After removal of the floating cells, the remaining attached cells were passed, harvested for protein or RNA, and analyzed.

Western Blot Analysis

I. Sample Harvest and Preparation

The cell culture of interest for protein analysis was harvested and lysed using 100-400µl of ice-cold 1X RIPA per 10cm dish (20 mM Tris-HCl pH 7.5, 150 mM NaCl, 1 mM Na_2EDTA, 1 mM EGTA, 1% NP-40, 1% sodium deoxycholate, 2.5 mM sodium pyrophosphate, 1 mM β–glycerophosphate, 1 mM Na_3VO_4, 1 µg/ml leupeptin) supplemented with complete, EDTA-free

protease inhibitors (Roche Diagnostics) and the proteasome inhibitor MG132 (EMD Millipore San Diego, CA, USA). Using a cell scraper, the cells were scraped and transferred to a microcentrifuge tube and snap frozen in liquid nitrogen. The samples were kept at -80°C until ready for analysis.

Each sample was then sonicated at an amplitude of 30 (Q700 Sonicator System, QSonica Sonicators, Newtown, CT). Samples were subjected to a cycle of 10 seconds of sonication followed by 30 seconds of rest on ice slurry, for a total of seven cycles (QSonica Microtip #4418, 1/8" Diameter). Samples were then centrifuged for 20 minutes at 15,000 RPM. 6μl of supernatant was removed and diluted 10-fold in 1X RIPA for use in the BCA assay (see below). The remainder of the supernatants were diluted in 5X loading dye and boiled for 5 minutes, placed on ice for 1 minute, and stored at -80°C.

II. Bicinchoninic Acid Assay (BCA Assay): Protein Quantification and Internal Controls

The Thermo Scientific Pierce BCA Protein Assay was utilized as a method to accurately quantify the total amount of protein present in a sample. Protein standards using bovine serum albumin (BSA) are prepared in order to quantify the sample protein concentrations based on the absorbance at 562nm.

In a 96-well plate, BSA standards diluted in 1X RIPA with concentrations of 0.5μg/ml, 0.25μg/ml, 0.125μg/ml, 0.0625μg/ml, and 0.03125μg/ml were prepared. One blank consisting of 1X RIPA was also prepared. Enough BCA working reagent was prepared in order for each sample, measured in duplicate, and each standard to have 200μl. 50 parts of BCA reagent A was mixed with 1 part of BCA reagent B. 200μl of working reagent was added to each well to be measured. 25μl of each sample to be measured, including the standards, was loaded into an

individual well and mixed thoroughly by pipetting (1:8 to the working reagent). The plate was incubated for 30 minutes at 37°C. The plate was read using a plate reader at 562nm.

To quantify the protein concentration of each sample, a standard curve of known BSA concentration vs. absorbance at 562 nm was generated. A computer-generated linear trend line was added, displaying the slope and y-intercept values. The unknown samples were adjusted for the value of the blank's absorbance and averaged for each replicate. Using the linear trend line, each unknown's absorbance value was solved for x, the protein concentration. The 10-fold dilution was accounted for, and the resulting value was multiplied by 1/40 to yield the appropriate loading volume for 40μg of protein for the western blot.

III. Sodium Dodecyl Sulfate-Polyacrylamide Gel Electrophoresis (SDS-PAGE) & Protein Transfer

The cell lysate samples were separated in an 8.5% acrylamide gel using polyacrylamide gel electrophoresis and subsequently subjected to immunoblotting. The completed gels were transferred to PVDF membranes (EMD Millipore) using an overnight wet transfer apparatus (Bio-Rad Laboratories, Hercules, CA, USA). The membranes were blocked using 5% bovine serum albumin (BSA) or 5% milk + 0.02% sodium azide (Sigma-Aldrich) and incubated overnight at 4°C with the primary antibody. The Clarity Western ECL Substrates (Bio-Rad Laboratories) were used 1:1 for immunodetection of HRP and imaged on a Chemidoc XRS+ imaging system (Bio-Rad Laboratories). A full summary of antibodies used as well as their dilutions can be found in table 2. To determine the relative expression of the target protein relative to the control protein β-actin, FIJI (ImageJ) software was used to perform densitometry analyses. The FIJI software determined density peaks for each protein band and calculated the area under each peak. The peak values for each β-Actin band were then used with the peak values for the target

protein bands to calculate a ratio that represented the change in expression of the protein of interest relative to β-Actin. This method allowed for the selection of only the target protein bands, however it did not allow for the standardization of background signaling that may have occurred proximal to each band.

Target	Primary/Secondary	Species	Catalog No.	Company	Lot No.	Dilution Factor
RUNX1	Primary	Rabbit	4336S	Cell Signaling	4	1:1000
RUNX1	Secondary	Goat Anti-Rabbit HRP	3140	ThermoFisher Scientific (Invitrogen)	SA245916	1:3000
PIK3CA	Primary	Rabbit	4249	Cell Signaling	9	1:1000
PIK3CA	Secondary	Goat Anti-Rabbit HRP	3140	ThermoFisher Scientific (Invitrogen)	SA245916	1:3000
PIK3R1	Primary	Rabbit	4257	Cell Signaling	6	1:1000
PIK3R1	Secondary	Goat Anti-Rabbit HRP	3140	ThermoFisher Scientific (Invitrogen)	SA245916	1:3000
HA TAG dCAS9	Primary	Rabbit	3724	Cell Signaling	8	1:1000
HA TAG dCAS9	Secondary	Goat Anti-Rabbit HRP	3140	ThermoFisher Scientific (Invitrogen)	SA245916	1:3000
β-Actin	Primary	Mouse	3700S	Cell Signaling	10	1:5000
β-Actin	Secondary	Goat Anti-Mouse HRP	31430	ThermoFisher Scientific (Invitrogen)	SD251027	1:5000

Table 2: Summary of antibodies and dilution factors used for western blot protocols.

shRNA Controls: Reporter Gene GFP Sorting and Puromycin Selection

To maintain an efficient and high-quality RUNX1 knockdown, the infected cells were sorted via FACS based on relative expression of the pGIPZ reporter gene TurboGFP. The cells were collected and resuspended in sterile PBS with 5% horse serum and DAPI (1:5000) and subsequently sorted and plated. GFP efficiency and cell vitality was checked 24 hours later (Figure 8). To further maintain RUNX1 knockdown, the sorted cells underwent a one-week period of puromycin selection. Normal media was replaced with media containing 2μg/mL puromycin. Cells expression the GIPZ plasmid will express both the shRNA as well as resistance

to the antibiotic puromycin. The media was replaced every 24 hours to remove any floating and dead cells and to replace with fresh media.

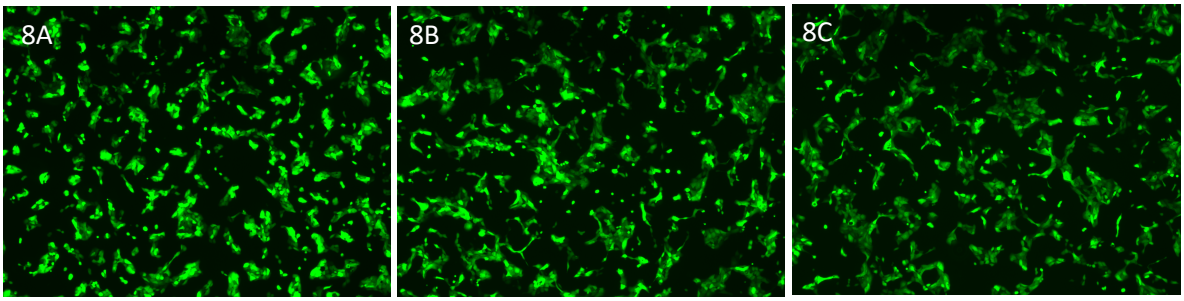

Figure 8: GFP Expression in MCF10A shRNA-Mediated Knockdown. Expression of the pGIPZ reporter gene GFP was analyzed using fluorescence microscopy to determine preliminary RUNX1 knockdown efficiency. Non-silencing shRNA (A), shRUNX1 C1 (B), and shRUNX1 C4 (C).

Quantitative PCR (qPCR)

RNA was harvested from cells and isolated with Trizol (Life Technologies). The samples were cleaned by DNase I digestion (Zymo Research, Irvine, CA, USA). RNA was reverse transcribed using SuperScript IV and random hexamers (Life Technologies). The cDNA was further cleaned with RNA removal via *E. coli* RNase H treatment (Life technologies). cDNA was then subjected to quantitative PCR using SYBR Green technology (Applied Biosystems, Foster City, CA, USA). The genes selected for qPCR analysis for this project were chosen based on unpublished ChIP-Sequencing data (Andrew Fritz) that first identified where in the genome RUNX1 binds. Additionally, unpublished RNA-sequencing data (Andrew Fritz) was used to determine the change in expression of genes upon RUNX1 depletion. This information, combined with genes known to drive BrCa (1), identified BrCa driver genes that may be under RUNX1 regulatory control due to proximal binding to the gene transcription start site and due to change in expression upon loss of RUNX1. A summary of primer sequence for these genes can be found in table 3.

Target	Forward Sequence	Reverse Sequence
SF3B1	GTGGGCCTCGATTCTACAGG	GATGTCACGTATCCAGCAAATCT
PIK3R1	ACCACTACCGGAATGAATCTCT	ACCACTACCGGAATGAATCTCT
KRAS	ACAGAGAGTGGAGGATGCTTT	TTTCACACAGCCAGGAGTCTT
FOXA1	GCAATACTCGCCTTACGGCT	TACACACCTTGGTAGTACGCC
PIK3CA	CCACGACCATCATCAGGTGAA	CCTCACGGAGGCATTCTAAAGT
TP53	CAGCACATGACGGAGGTTGT	TCATCCAAATACTCCACACGC
PTEN	TGGATTCGACTTAGACTTGACCT	GGTGGGTTATGGTCTTCAAAAGG
USP9X	TCGGAGGGAATGACAACCAG	GGAGTTGCCGGGGAATTTTCA
ATM	ATCTGCTGCCGTCAACTAGAA	GATCTCGAATCAGGCGCTTAAA
APC	AAAATGTCCCTCCGTTCTTATGG	CTGAAGTTGAGCGTAATACCAGT
PBRM1	AGGAGGAGACTTTCCAATCTTCC	CTTCGCTTTGGTGCCCTAATG
BUB1B	AAATGACCCTCTGGATGTTTGG	GCATAAACGCCCTAATTTAAGCC
GAPDH	TGTGGTCATGAGTCCTTCCA	ATGTTCGTCATGGGTGTGAA
RUNX1	AACCCTCAGCCTCAGAGTCA	CAATGGATCCCAGGTATTGG
CDH1	GGAAGTCAGTTCAGAGCATC	AGGCCTTTTGACTGTAATCACACC
ACTIN-B	AGCACAGAGCCTCGCCCTT	CGGCGATATCATCATCCA
N-CADHERIN	TGTTTGACTATGAAGGCAGTGG	TCAGTCATCACCTCCACCAT
VIMENTIN	AGGAAATGGCTCGTCACCTTCGTGAATA	GGAGTGTCGGTTGTTAAGAACTAGAGCT

Table 3: Summary of primer sequences used for quantitative PCR protocols.

Results

The central objective of this project was to first develop a RUNX1 loss of function model in human BrCa cells (10A and AT1) using inducible CRISPRi and shRNA. Upon RUNX1 loss, this study aimed to investigate how RUNX1 may be involved in the expression of predicted BrCa driver genes based on preliminary RUNX1 ChIP-seq data, RNA-seq data, and the published literature identifying BrCa driver genes (1). The long-term goal of this project is to therefore identify BrCa driver genes putatively regulated by the tumor suppressor action of RUNX1.

Doxycycline-Induced CRISPRi Knockdown of RUNX1

Previous work carried out by Alexandra Ojemann in the Stein/Lian laboratory successfully isolated stable clonal populations of AT1 cells infected with the CRISPRi-dCas9-KRAB system. Upon addition of varying concentrations of the antibiotic doxycycline to cells in culture, dCas9 expression at the protein level was determined among four sets of clones denoted as clones 1, 4, 5, and 6. Doxycycline induction was carried out for three days with concentrations of 2μM, 5μM, and 10μM. In response to doxycycline, dCas9 was expressed at the protein level, as determined by western blot analysis (Figure 9). The uninduced samples (doxycycline = 0μM) were found to express no dCas9 (Figure 9).

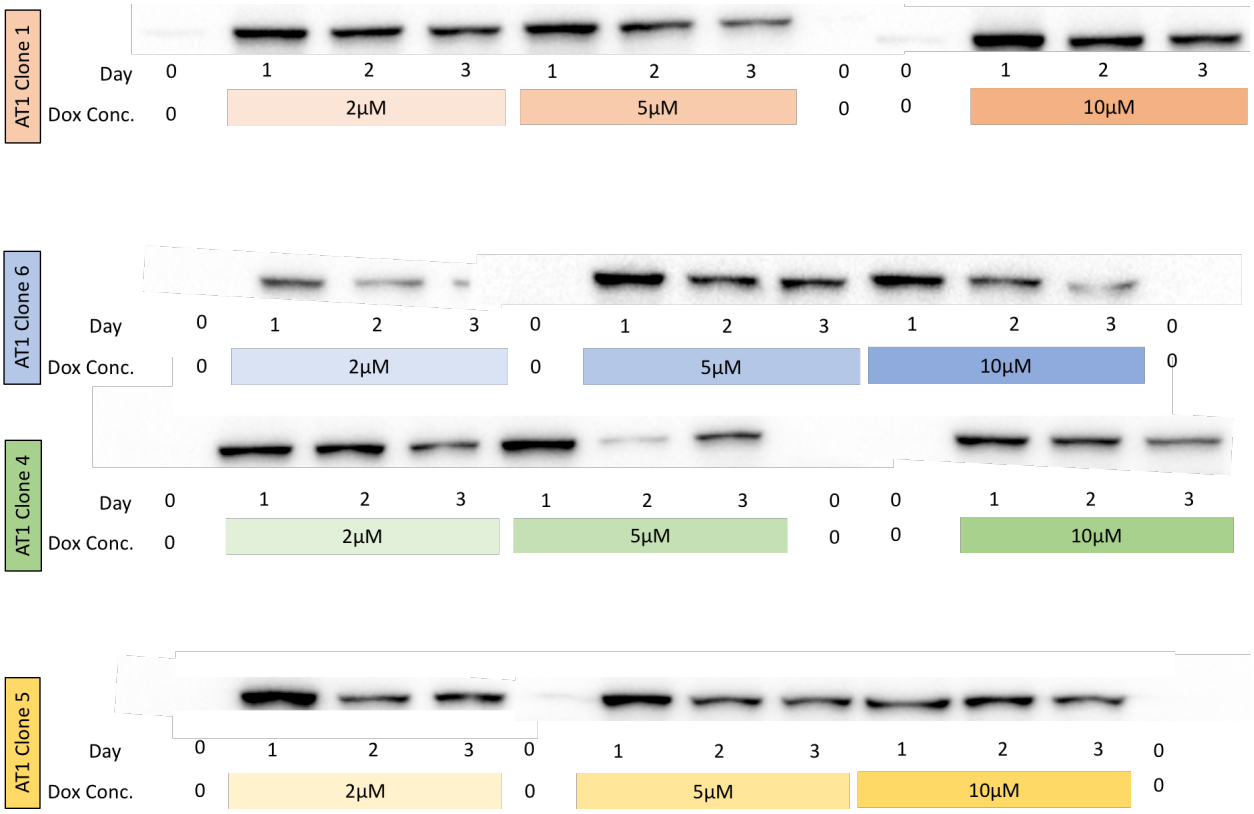

Figure 9: Upon Dox-Induction, AT1 Cells Transfected with CRISPRi Plasmid pLV hU6-sgRNA hUbC-dCas9-KRAB-T2a-GFP Expressed dCas9. dCas9 was expressed at the protein level in AT1 clones 1, 4, 5 and 6. Dox concentrations of 2μM, 5μM, and 10μM all demonstrated dCas9 expression. Standard western blot protocol was followed, and the antibody used was HA Tag 3724 Lot #8 Rabbit mAb (Cell Signaling).

Relative to β-Actin expression, which was used as an internal control, dCas9 expression among the AT1 clones did not directly correlate with doxycycline concentration. Higher doxycycline concentration did not consistently result in a greater expression in dCas9 (Figure 10). In some AT1 clones, 2μM doxycycline was just as, or more, effective in inducing dCas9 expression than 10μM doxycycline. A complete summary of dCas9 expression at the protein level upon the addition of doxycycline over the course of three days is included in Table 4.

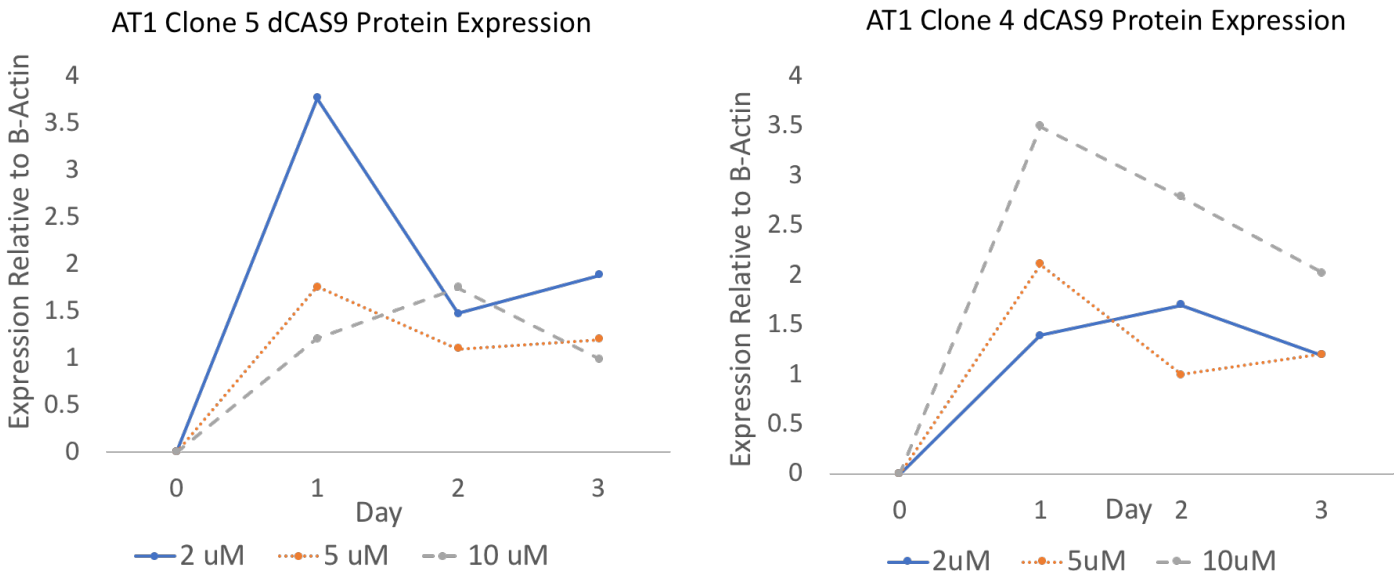

Figure 10: Doxycycline Concentration and dCas9 Expression do not Directly Correlate. Varying concentrations of doxycycline resulted in varying levels of dCas9 expression in AT1 clone 5 (7A) as well as AT1 clone 4 (7B) at the protein level. Expression was determined via western blot analysis relative to β-actin expression. One western blot was analyzed for each clone for each of three doxycycline concentrations.

MCF10AT1	Timepoint (Day)	Doxycycline [uM]	dCAS9 Signal > 1.0	dCAS9 Expression (relative to B-Actin)
Clone 1	1	2	✓	1.4
		5	✓	1.9
		10	✓	2.6
	2	2	✓	1.3
		5	✓	1.3
		10	✓	1.8
	3	2	✓	1.0
		5	✗	0.8
		10	✓	1.6
Clone 4	1	2	✓	1.4
		5	✓	2.1
		10	✓	3.5
	2	2	✓	1.7
		5	✓	1.0
		10	✓	2.8
	3	2	✓	1.2
		5	✓	1.2
		10	✓	2.0
Clone 5	1	2	✓	3.8
		5	✓	1.8
		10	✓	1.2
	2	2	✓	1.5
		5	✓	1.1
		10	✓	1.8
	3	2	✓	1.9
		5	✓	1.2
		10	✗	0.9
Clone 6	1	2	✗	0.6
		5	✓	1.4
		10	✓	2.6
	2	2	✗	0.1
		5	✓	1.3
		10	✗	0.7
	3	2	✗	0.0
		5	✓	1.8
		10	✓	1.0

Table 4: Doxycycline-Induced AT1 Clones Expressed dCas9 Protein. Upon addition of 2µM, 5µM, and 10µM doxycycline, AT1 clones 1,4,5 and 6 expressed dCas9 at the protein level. Doxycycline was replenished every 24 hours for 72 hours total. Standard western blot protocol was followed, and **β**-Actin served as a control. Using FIJI software, densitometry analysis was performed to yield the expression of the dCas9 signal relative to β-Actin. HA Tag (dCas9) Primary Antibody: Rabbit mAb HA Tag #3724 Lot 8 (Cell Signaling). β-Actin Primary Antibody: β-Actin Mouse mAb #3700S Lot 10 (Cell Signaling)

Further AT1 clonal analysis was carried out to determine RUNX1 protein expression in each of the four clones expressing dCas9 upon dox-induction. The first round of CRISPRi-mediated RUNX1 knockdown demonstrated a clear need for CRISPRi optimizations. Among AT1 clonal populations expressing the dCas9 plasmid, RUNX1 expression at the protein level varied drastically between doxycycline concentrations and between consecutive days after infection with the sgRNA CRISPRi guides targeting RUNX1 (Figure 11). A consistent knockdown trend was not seen throughout the three days of doxycycline induction in any of the clones or at any specific doxycycline concentration (Figure 12).

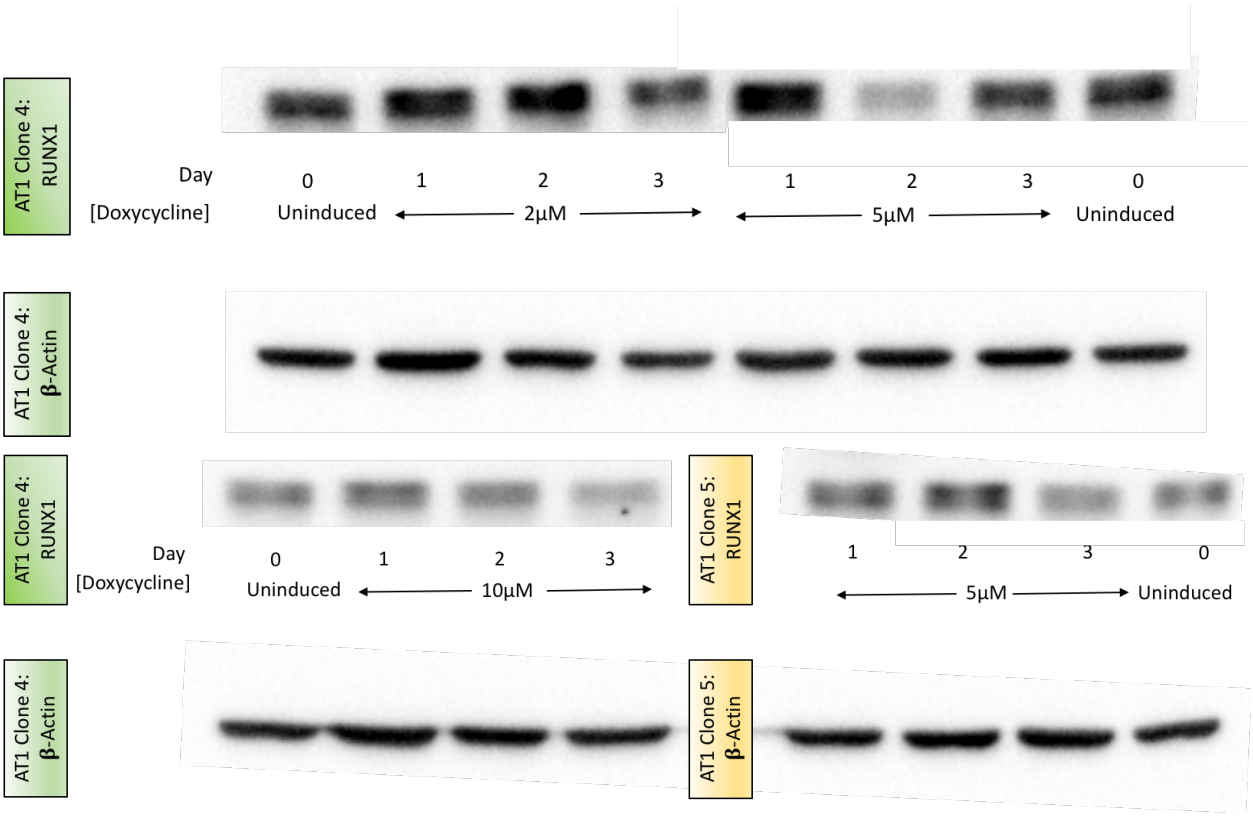

Figure 11: Upon Dox-Induction, AT1 Cells Infected with CRISPRi Plasmid pLV hU6-sgRNA hUbC-dCas9-KRAB-T2a-GFP Expressed Variable Levels of RUNX1. AT1 clones 4 and 5 expressed varying levels of RUNX1 at the protein level upon three days of doxycycline induction of varying concentrations. Standard western blot protocol was followed. The RUNX1 antibody used was AML1 Rabbit mAb #4336S Lot 4 (Cell Signaling). β-Actin served as a control, mouse mAb #3700S Lot 10 (Cell Signaling).

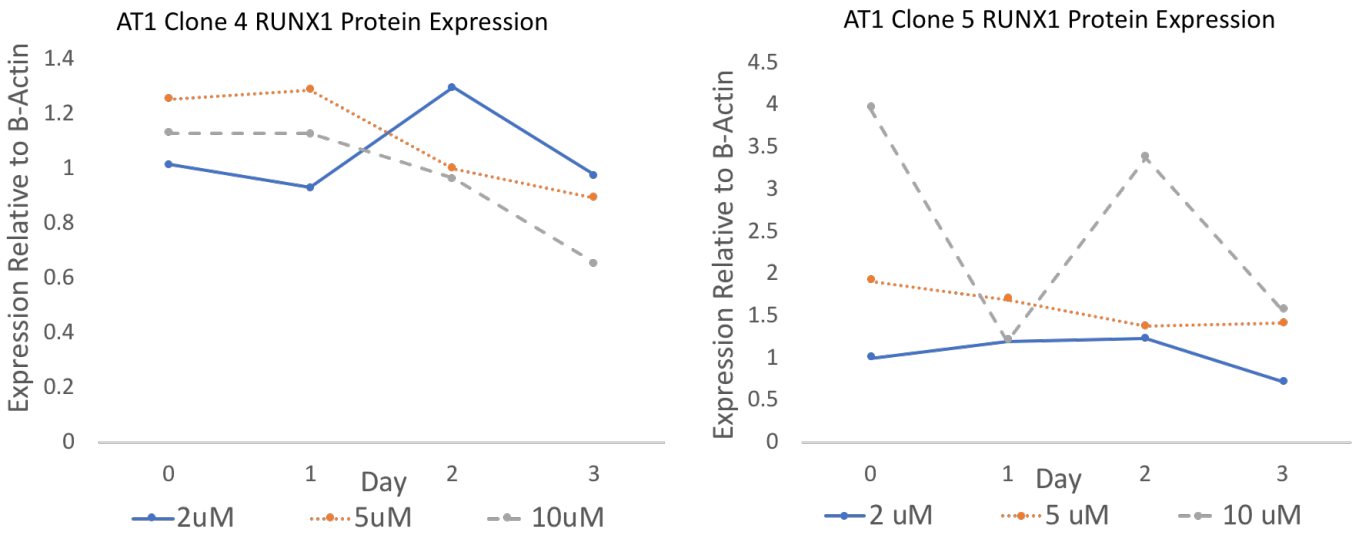

Figure 12: Upon Dox-Induction, AT1 Cells Infected with CRISPRi Expressed Variable Levels of RUNX1. AT1 clones 4 (10A) and 5 (10B) expressed varying levels of Runx1 at the protein level upon three days of doxycycline induction of concentrations 2μM, 5μM, and 10μM. Standard western blot protocol was followed and the RUNX1 antibody used was AML1 Rabbit mAb #4336S Lot 4 (Cell Signaling). β-Actin served as a control, mouse mAb #3700S Lot 10 (Cell Signaling).

Based on the variability of RUNX1 knockdown, the CRISPRi-dCas9 system was optimized at the level of the virus production and the subsequent infection of the AT1 cells. We hypothesized that increasing the quantity of virus would result in a more efficient and consistent gene knockdown.

Increasing the Virus Titer of CRISPRi Targeting RUNX1 Yielded Greater Knockdown Efficiency

In order to gain a more significant and consistent knockdown of RUNX1 upon the addition of doxycycline, the virus titer containing the sgRNA targeting RUNX1 was increased five-fold. We hypothesized that a higher virus titer would result in a better knockdown of RUNX1, as the infection efficiency would likely increase. Based on previous clonal protein expression of RUNX1, clone 4 was selected to test the high virus titer CRISPRi knockdown. In previous experiments, AT1 clone 4 was the only clone that displayed a consistent downward trend of RUNX1 expression as the time progressed (Figure 12). Therefore, clone 4 was theorized

to best show RUNX1 depletion upon infection with a five-fold increase in virus. After infection of the sgRNA RUNX1 guides and upon addition of 2μM doxycycline every 24 hours for three days, AT1 clone 4 displayed an appreciable net loss of RUNX1 at the protein level (Figure 13). Samples were run in duplicate, generating a standard error of the mean. Replicate A demonstrated a consistent and significant depletion in RUNX1 as time progressed, while Replicate B showed RUNX1 depletion on days one and three with an increase in RUNX1 expression on day two, relative to β-actin (Figure 14). However, this is also true for the non-induced control of 0μM doxycycline (Figure 14). In both control replicates, RUNX1 expression increased on day two and decreased again on day three (Figure 13, Figure 14). A potential consideration for this result is that RUNX1 may exert a compensatory mechanism to combat the repressive effects on the inducible CRISPRi dCas9-KRAB system to therefore maintain adequate expression of RUNX1 in the cells, though additional biological replicates must be carried out to fully investigate this finding.

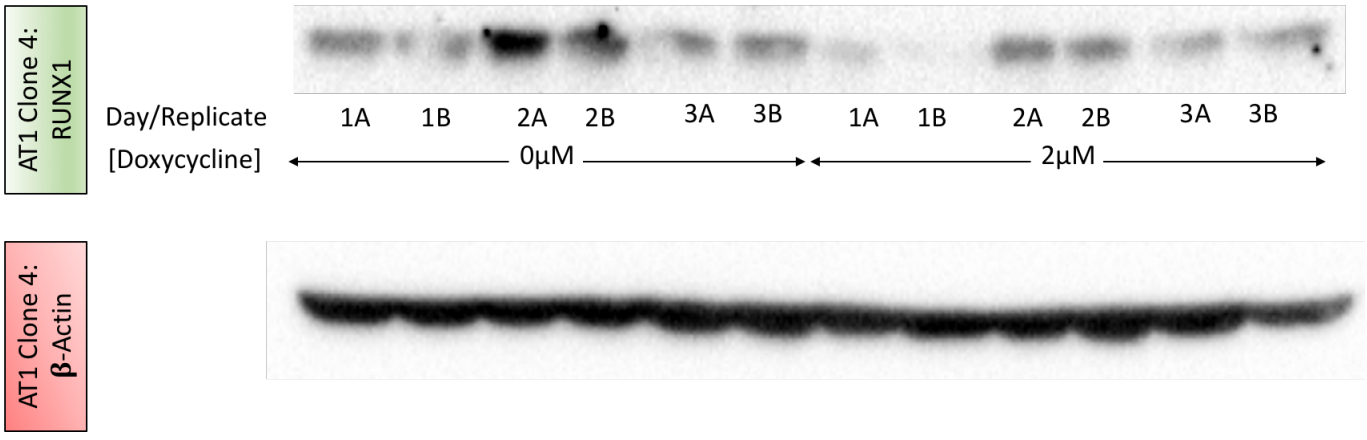

Figure 13: Doxycycline-Induced RUNX1 CRISPRi Knockdown in MCF10AT1 Clone 4 cells. RUNX1 expression was analyzed via Western Blot analysis. Two replicates of AT1 cells were carried out and 2μM Doxycycline was added every 24 hours for a 72-hour period. Samples were harvested every 24 hours using 1X RIPA and standard RUNX1 Western Blot protocol was followed. RUNX1 antibody used: AML1 Rabbit mAb #4336S Lot 4 (Cell Signaling). β-Actin served as a control mouse mAb #3700S Lot 10 (Cell Signaling).

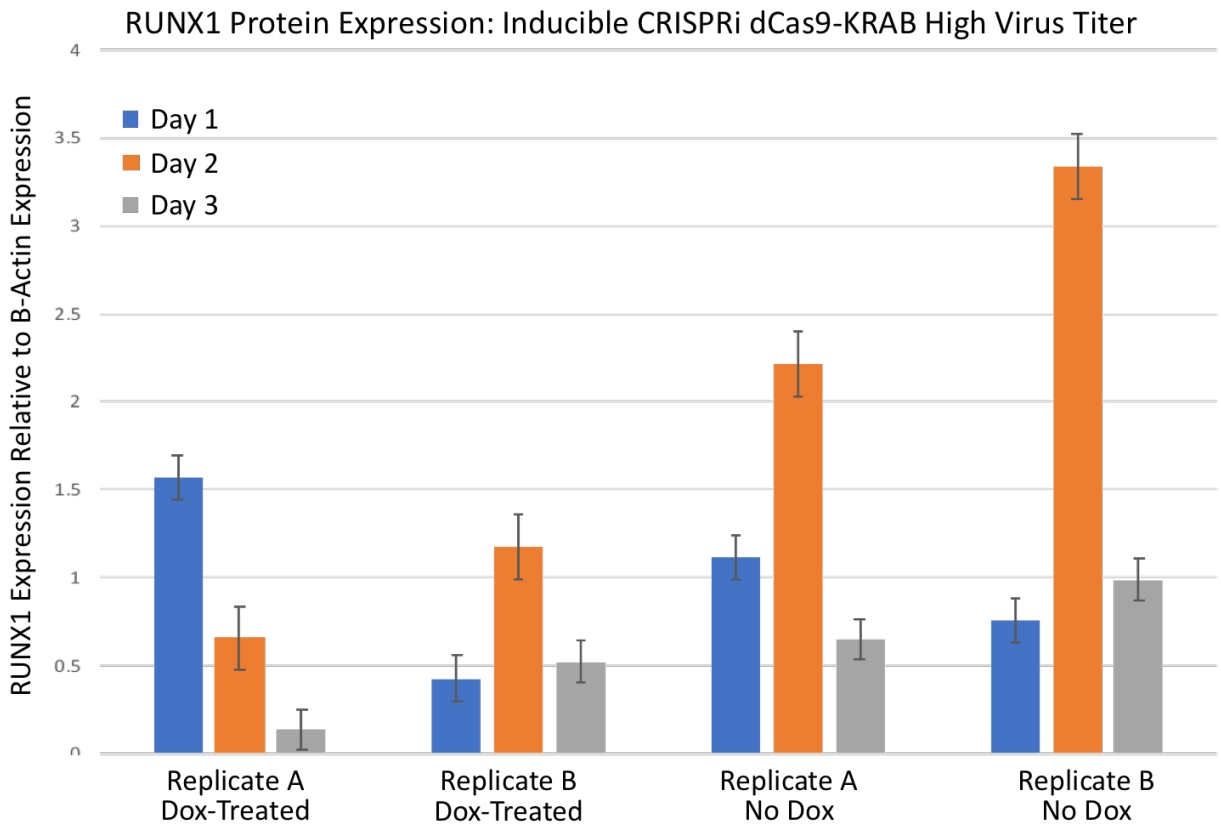

Figure 14: Doxycycline-Induced RUNX1 CRISPRi Knockdown in MCF10AT1 Clone 4 cells (Viral Construct 5). RUNX1 protein expression was analyzed via Western Blot and quantified in relation to β-actin expression. Two replicates of AT1 cells were performed and 2μM Doxycycline was added every 24 hours for a 72-hour period. Samples were harvested every 24 hours using 1X RIPA and standard RUNX1 Western Blot protocol was followed. Using FIJI software, densitometry analysis was performed to yield the expression of the RUNX1 signal relative to β-Actin. Error bars represent the standard error of the mean (SEM).

In four AT1 clonal populations previously developed by Alexander Ojemann of the Stein/Lian group, dCas9 was expressed upon doxycycline-induction as early as 24 hours and at a concentration as low as 2μM (Table 4). dCas9 expression therefore confirmed successful transfection of the dCas9-KRAB plasmid and allowed for dox-induced RUNX1 gene silencing studies to be performed. Initial doxycycline induction in AT1 clone 4 did not yield significant knockdown of RUNX1, as RUNX1 expression was highly variable between 24-hour harvest

points and between doxycycline concentrations used for induction (Figure 14). To optimize the inducible CRISPRi system, five times the quantity of virus carrying the sgRNA guides targeting RUNX1 was generated in HEK293T cells. Upon infection, RUNX1 knockdown improved compared to previous studies, but did not show consistency or validity compared to the uninduced control samples (Figure 14). For these reasons, and due to time constraints, the CRISPRi-mediated knockdown system was no longer pursued, and we began developing a RUNX1 knockdown system using shRNA in order to perform downstream genomic analyses in cells depleted of the RUNX1 transcription factor.

shRNA-Mediated Knockdown of Runx1

A second gene knockdown tool, shRNA, was utilized in the 10A series in order to gain a more complete and consistent depletion of RUNX1. The shRNA system has proven effective and

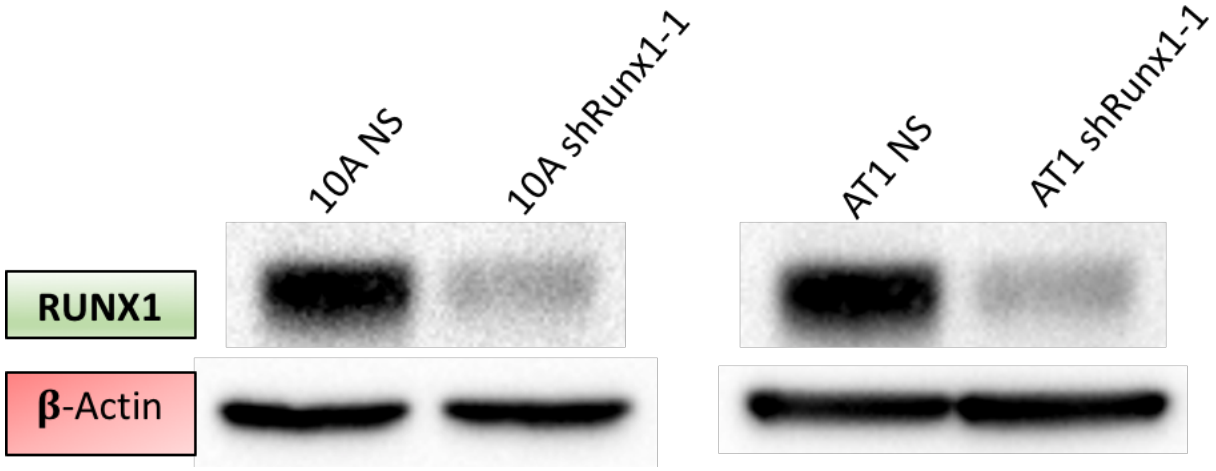

Figure 15: Protein expression profile of MCF10A and MCF10AT1 upon shRNA knockdown targeting RUNX1. GFP^+ 10A and AT1 cells were selected for via FACS and standard western blot protocol for RUNX1 was followed. NS: shRNA non-silencing construct. shRUNX1-1: shRNA RUNX1 knockdown construct. RUNX1 AML1 Rabbit mAb #4336S Lot 4 (Cell Signaling) β-Actin served as a control mouse mAb #3700S Lot 10 (Cell Signaling).

successful in our lab and was therefore the method of choice to mediate RUNX1 depletion in a timely manner (3).

Knockdown of RUNX1 in both 10A and AT1 cells by shRNA proved effective at the protein level. Western blot analysis determined that RUNX1 was decreased over 70% relative to the non-silencing shRNA in both the 10A and AT1 cells (Figure 15, Figure 16).

Short hairpin RNA knockdown also proved efficient at the RNA level. qPCR was carried out for cDNA of shRunx1 AT1 cells to determine the RNA expression of RUNX1 as well as E-cadherin (CDH1) following depletion of RUNX1. Expression change relative to the housekeeping

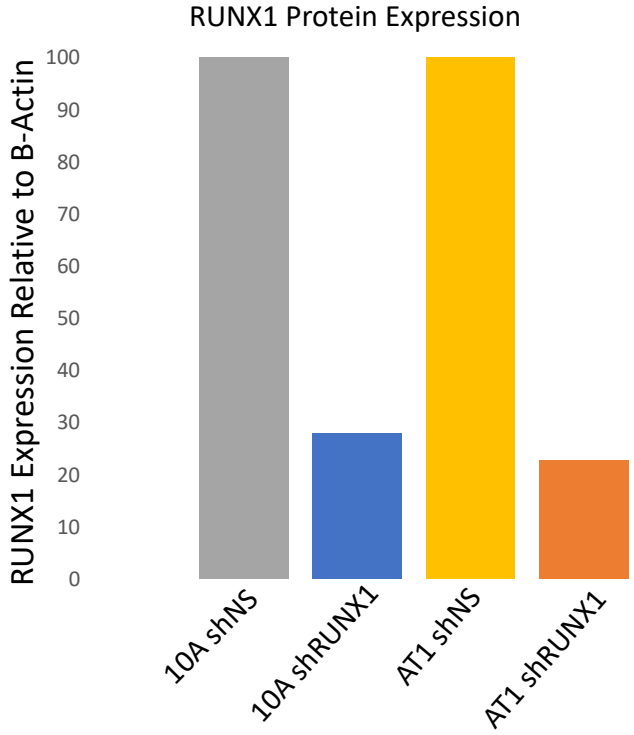

Figure 16: RUNX1 protein expression change upon shRUNX1 knockdown in 10A and AT1 cells. Relative to **β**-Actin, RUNX1 was depleted by 72% in 10A cells (n=1) and 77% in MCF10AT1 cells (n=1) using shRUNX1-1. NS: shRNA non-silencing construct. shRUNX1-1: shRNA RUNX1 knockdown construct. Using FIJI software, densitometry analysis was performed to yield the expression of the RUNX1 signal relative to β-Actin.

gene glyceraldehyde 3-phosphate dehydrogenase (GAPDH) as well as the non-silencing (NS) construct yielded ΔΔCT values for gene expression of RUNX1 and CDH1. Fold expression change was calculated by raising (-ΔΔCT) to the power of 2. In AT1 cells, RUNX1 depletion resulted in a loss of the epithelial marker CDH1, lending further support to previous findings that RUNX1 loss advances the mesenchymal phenotype and EMT (Figure 17).

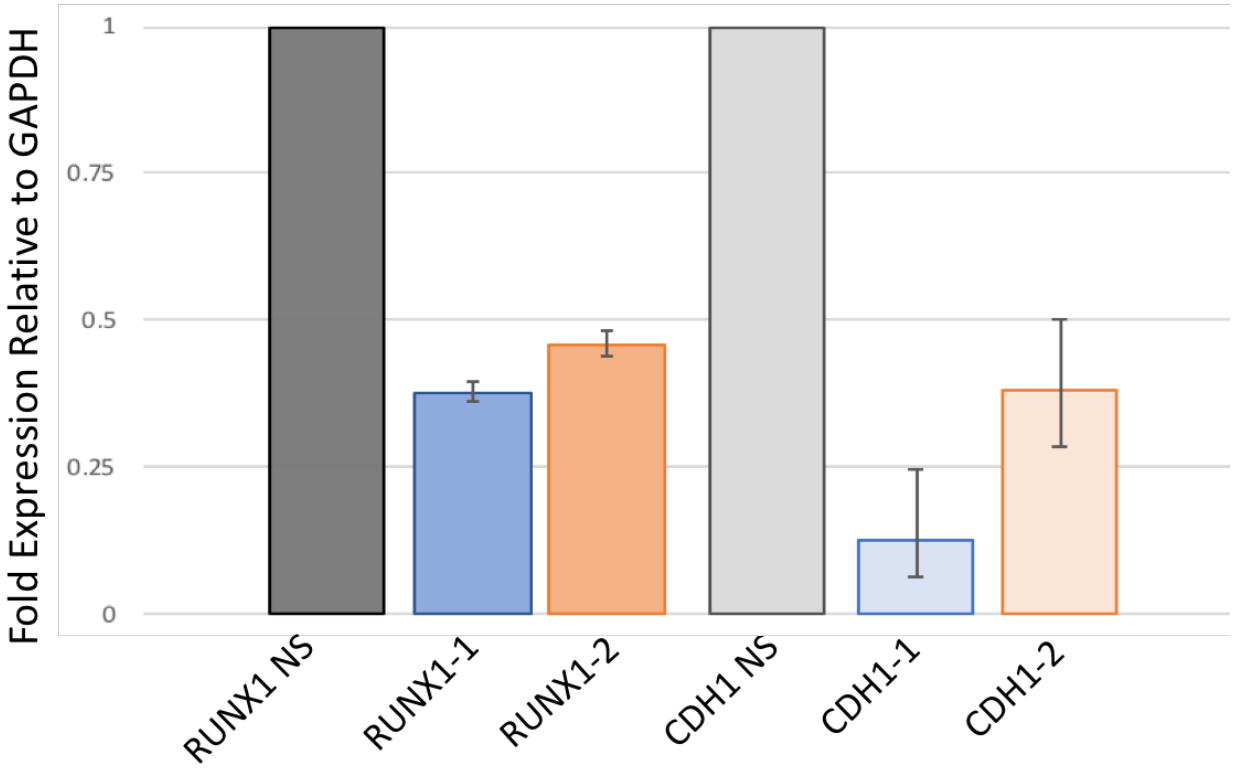

Figure 17: shRNA-Mediated Knockdown of RUNX1 Decreases CDH1 Expression at the RNA Level in AT1 Cells. Upon shRNA-mediated knockdown of RUNX1, qPCR analysis determined that CDH1 decreased at the mRNA level. Gene expression levels are relative to GAPDH as well as the non-silencing (NS) shRNA construct. Error bars represent SEM. qPCR was run in duplicate for two biological replicates.

To investigate the role of RUNX1 as a tumor suppressor, potential BrCa driver genes were identified using unpublished ChIP-seq and RNA-seq data from the Stein/Lian lab (Andrew Fritz). The ChIP-seq data identified where in the genome RUNX1 is normally bound, while the RNA-seq data identified the change in expression of genes upon RUNX1 depletion. Together

with this, as well as data published from Serena Nik-Zainal and colleagues (1), we identified top BrCa driver genes with transcription start sites that RUNX1 proximally binds to and that RUNX1 may exert regulatory control over (Table 5). This yielded a list of 11 BrCa driver genes that change in expression upon RUNX1 depletion and contain transcription start sites at which RUNX1 binds.

Breast Cancer Driver Gene of Interest	Distance from RUNX1 Binding to Gene TSS (bp)	Change in Expression Upon Loss of RUNX1
SF3B1	0	1.287
PIK3R1	410	1.539
PIK3CA	48046	1.744
KRAS	0	1.700
FOXA1	0	1.737
TP53	579	0.825
USP9X	406	1.208
ATM	0	1.566
APC	0	2.186
PBRM1	0	1.264
BUB1B	44925	2.900

Table 5: Based on whole-genome analysis of 1,332 breast cancers, driver genes based on mutation frequency were found (1). Subsequent analysis based on driver gene rating, distance from gene TSS to RUNX1 binding, and change in expression upon RUNX1 depletion generated a subset of BrCa driver genes that may be under the control of RUNX1.

After successful depletion of RUNX1 in 10A and AT1 cells using shRNA, the regulatory action of RUNX1 on these specific BrCa driver genes was investigated. Phosphatidylinositol-4,5-Bisphosphate 3-Kinase Catalytic Subunit Alpha (PIK3CA) and Phosphoinositide-3-Kinase Regulatory Subunit 1 (PIK3R1) are two kinase protein components that are part of the same kinase protein complex and that were determined to be commonly mutated in BrCa and therefore identified as BrCa driver genes (1). Upon RUNX1 depletion, the RNA and protein expression profiles of these specific kinases were analyzed to determine if PIK3CA and PIK3R1 are under the regulatory control of RUNX1. qPCR data revealed that RUNX1 knockdown resulted in an increase in both PIK3CA and PIK3R1 RNA expression compared to non-silencing (Figure 18). At the protein level, RUNX1 depletion in AT1 cells resulted in an increase in PIK3CA

(Figure 19). Conversely, RUNX1 depletion did not significantly alter the protein expression of PIK3R1 (data not shown).

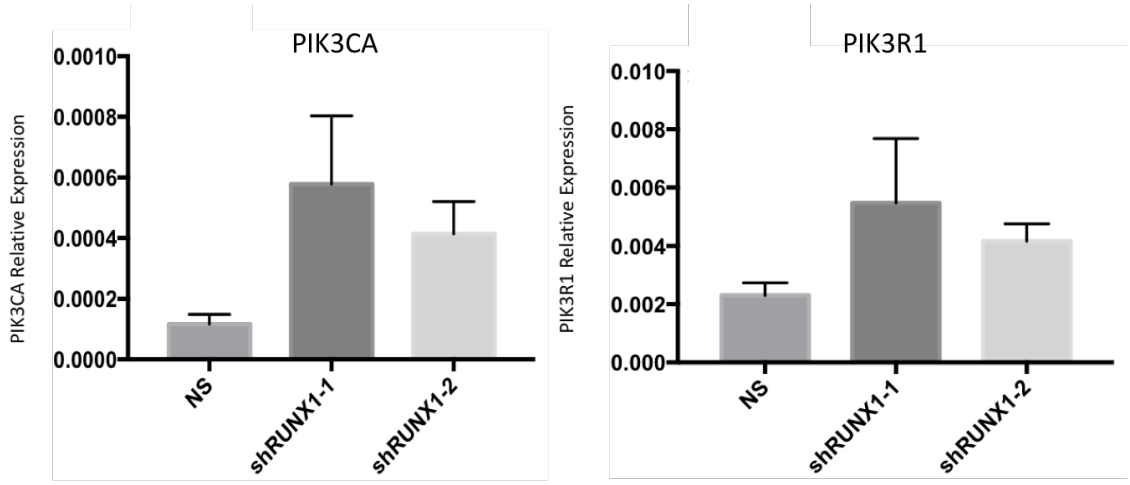

Figure 18: Expression of PIK3CA/R1 Increased upon RUNX1 Knockdown in 10A Cells. qPCR determined that upon shRNA knockdown of RUNX1 in 10A cells there was an increase in PIK3CA and PIK3R1 mRNA expression, suggesting a role for RUNX1 in regulating PI3K kinase functions in BrCa. Error bars represent the SEM. NS: shRNA non-silencing construct. shRUNX1-1: shRNA RUNX1 knockdown construct 1. shRUNX1-2: shRNA RUNX1 knockdown construct 2.

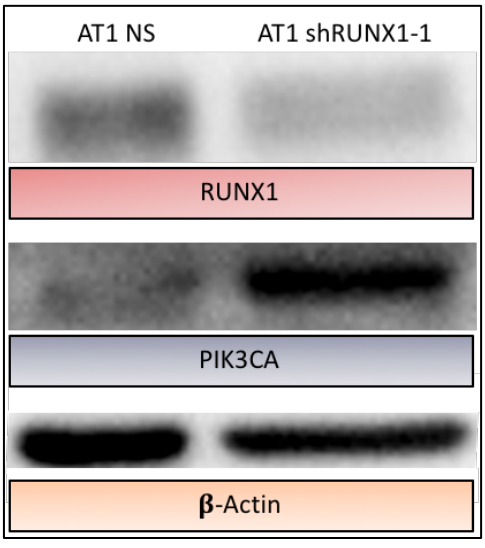

Figure 19: Expression of PIK3CA protein increased upon RUNX1 knockdown in AT1 cells. Western blot analysis determined that upon shRNA knockdown of RUNX1 in AT1 cells there was an increase in PIK3CA protein expression, suggesting RUNX1 exerts regulatory action on PIK3CA's function in BrCa. Standard western blot protocol was followed, and β-Actin served as a control. NS: shRNA non-silencing construct. shRUNX1-1: shRNA RUNX1 knockdown construct. Primary antibodies used: RUNX1 AML1 Rabbit mAb #4336S Lot 4 (Cell Signaling); PIK3CA Rabbit mAb #4249 (Cell Signaling); β-Actin Mouse mAb #3700S Lot 10 (Cell Signaling).

The shRNA knockdown system targeting RUNX1 proved effective in depleting RUNX1 at the transcriptomic level. In 10A and AT1 cell models, representing both normal-like and tumor-like cells, RUNX1 was decreased by approximately 70% (Figure 16). This level of RUNX1 depletion resulted in a decrease in RNA expression of the epithelial marker E-cadherin (Figure 17) and an increase in the RNA expression of PIK3R1 (Figure 18) and an increase in both the RNA and protein expression of PIK3CA (Figure 18, Figure 19). These preliminary results suggest that RUNX1 may exert regulatory control over the PI3K signaling pathway in a repressive manner, since upon depletion the expression of PI3K kinase proteins increased in both 10A and AT1 cells. These findings were found in duplicate (n=2) for RNA expression of PIK3CA and PIK3R1 in 10A cells, while the findings for PIK3CA protein expression in AT1 cells were found in one biological replicate of shRNA-mediated RUNX1 depletion.

Discussion & Future Directions

Loss-of-function studies are instrumental in advancing our knowledge of how a gene exerts regulatory control in the cell. There is evidence that RUNX1 may act as a tumor suppressor gene through its action as a transcription factor and master regulator of various cellular pathways that are critical to cellular development, survival, growth and proliferation (3, 4, 45). In this project, two systems were utilized to generate a loss of RUNX1 function in the MCF10 BrCa cell series; inducible CRISPRi-dCas9-KRAB and shRNA.

Inducible CRISPRi is one of the most well-known genome editing tools in scientific research today. The precision, stability and reproducibility of the system make it a premier option for use in gene activation or inhibition studies. In this study, inducible CRISPRi optimizations and successive trials did not produce a RUNX1 knockdown sufficient for

downstream analyses. This, in concert with time constraints, led us to utilize the shRNA system for knockdown of RUNX1. However, it may be the case that the inducible CRISPRi system has its own limitations depending on the target gene. It was demonstrated here that across multiple clonal populations, cells expressed adequate dCas9 protein for multiple days across multiple concentrations of doxycycline (Table 4). The expression of dCas9 is a key indicator that the inducible system has been acquired by the cell and is a good indication of possible gene knockdown. However, a serious concern for inducible CRISPRi that targets RUNX1 is the fact that the RUNX1 gene is regulated by two different promoters known as P1 and P2, each of which contributes to the overall expression of RUNX1. Additionally, the promoters P1 and P2 function differently in different cell types. We designed guides for both P1 and P2, three guides per promoter for a total of six guides (Table 1). Therefore, in order for the CRISPRi system to be effective in generating an appreciable knockdown of at least 80%, gene silencing at both promoters P1 and P2 must be achieved. This requirement was likely a limitation for the CRISPRi system, as failure of gene knockdown at just one promoter would allow for RUNX1 expression. This addresses a major hurdle facing loss-of-function studies, as it can be much more difficult to generate a complete silencing of a gene compared to hyper activating or overexpressing a gene.

A theoretical limitation of this study may lie within the fact that RUNX1 is a true master regulator in the breast epithelial cells. Even as the CRISPRi experiment was optimized, either by clonal selection for high dCas9 expression, or by increasing the virus titer, adequate knockdown was not consistently achieved. It may be possible that RUNX1 holds a compensatory or reserve mechanism to ensure its expression, as it is vital to many processes within the cell including signaling pathways, growth and proliferation, cell survival and DNA damage response (4).

Similarly, this is plausible since CRISPRi utilizes a deactivated Cas9 in place of Cas9 and does not exert nuclease activity on the target gene. It is therefore a matter of steric interference via the KRAB repression domain that blocks transcription, not permanent gene excision as seen in the classical CRISPR-Cas9 model. This system is therefore developed to create a non-permanent loss of RUNX1. For that reason, RUNX1 may be able to exert a compensatory mechanism that results in decreased efficiency for dCas9-KRAB binding and transcriptional silencing in the cell.

Conversely, perhaps the CRISPRi system is ineffective in targeting RUNX1 at the genomic level because doing so activates apoptotic events in the cell. Apoptotic studies were not performed in this project, though it may be important to determine if RUNX1 repression at the genomic level in BrCa is too catastrophic for the cell, leading to apoptotic events for the population of cells that the CRISPRi system was successful. These events would therefore only leave behind the population of cells for which RUNX1 expression was not repressed, as seen in this project.

Other CRISPRi limitations may simply lie within the optimization of the experimental set up. We found that increasing the virus titer and raw production of the virus five-fold yielded a more efficient knockdown (Figure 14). Further optimization with an even higher virus titer could therefore be conducted to generate sufficient knockdown of RUNX1. Additionally, this project only utilized a total of six CRISPRi guides (Table 1). Three guides were designed to target RUNX1 promoter 1 and three guides were designed to target RUNX1 promoter 2. The online CRISPR design tool, Benchling, was utilized in the design of these guides and therefore they should contain the necessary parameters for effective knockdown. However, as these guides

did not prove very effective, a new set of guides may need to be designed for successful knockdown. Due to time constraints for this project, we did not pursue generating new guides.

shRNA-mediated depletion of RUNX1 proved to be an effective method of knocking down RUNX1 expression at the protein level as well as at the RNA level (Figure 15, Figure 16). shRNA targeting RUNX1 was previously performed in our laboratory (3) and was therefore a dependable choice for a knockdown system when facing time constraints. At the protein level, RUNX1 was knocked down approximately 75% in both the 10A and AT1 cell line. qPCR of two replicates in AT1 cells also identified a significant reduction in expression of RUNX1 at the RNA level upon shRNA knockdown (Figure 17). These results allowed for further analyses of the tumor suppressor role of RUNX1 in BrCa.

Quantitative PCR first validated the role of RUNX1 in maintaining the epithelial phenotype by preventing EMT as first demonstrated by Hong and colleagues (3). We found that in AT1 cells across two replicate samples, a reduction of RUNX1 RNA expression resulted in a dramatic decrease of the RNA expression of the epithelial marker E-cadherin, as compared to the non-silencing shRNA control (Figure 17). This lends evidence in support of the tumor suppressor role of RUNX1 in BrCa, as maintenance of the epithelial phenotype and prevention of EMT are essential in preventing cancer progression and aggression.

Most notably, we determined that upon depletion of RUNX1, there was a clear increase in PIK3CA and PIK3R1 expression at the RNA level in 10A cells (Figure 18). At the protein level, an increase in PIK3CA expression was found upon RUNX1 depletion in AT1 cells (Figure 19). PIK3CA and PIK3R1 are genes of the phosphatidylinositol-3-kinase (PI3K) pathway that are commonly mutated in human cancers (27). PI3K signaling is a critical pathway involved in both

normal and malignant cellular processes including cell growth, proliferation and apoptosis (Figure 20) (46). Notably, the PIK3CA gene has been found to be mutated in more than one-third of breast cancers (27). Additionally, one study determined that 9% of the study's cohort of breast cancer patients harbored both PIK3CA and PIK3R1 mutations that resulted in hyperactivity of the PI3K pathway and oncogenesis (47).

Using an unpublished ChIP-Seq data set that identified where the RUNX1 protein is bound throughout the genome (Andrew Fritz), PIK3R1 was identified as a BrCa driver gene that RUNX1 binds proximal to the transcription start site (Table 5). Similarly, PIK3CA was identified as a BrCa driver gene that RUNX1 binds, though less proximal than the transcription start site of PIK3R1. Unpublished RNA-seq data (Andrew Fritz) also determined that upon RUNX1 depletion, PIK3CA and PIK3R1 are upregulated in expression (Table 5). RUNX1 regulatory control of PIK3CA may therefore occur via distant enhancers or genomic lopping domains, while RUNX1 control of the PIK3R1 gene may occur at the transcription start site. It was confirmed that upon RUNX1 knockdown in BrCa, there is a significant increase in expression of PIK3CA and PIK3R1 compared to the non-silencing sample which expressed RUNX1 protein and RNA. Although PIK3CA and PIK3R1 are among the most commonly mutated genes in breast cancer, it is the difference between the non-silencing vector and the shRNA vector truly targeting RUNX1 that demonstrates the regulatory control of RUNX1 on these important PI3K pathway oncogenic genes. Since RUNX1 exerts regulatory control with a myriad of genes involved in growth and development, the negative regulation of PIK3CA and PIK3R1 may therefore be direct or indirect.

The PI3K pathway is vast, exerting control over and interacting with components including AKT, mTOR, RAS, VEGF, and EGF, all of which have roles in cell growth, survival, proliferation, morphology, apoptosis, migration and adhesion (Figure 20) (9, 48). For these reasons, hyperactivation of PIK3CA and PIK3R1 upon loss of RUNX1 may be a critical part of cancer progression toward metastasis and invasion, ultimately resulting in poor patient prognosis. Moreover, the high frequency of PIK3CA mutations in BrCa has focused on PIK3CA inhibition as a novel clinical target and potential drug scheme for BrCa treatment (49). RUNX1

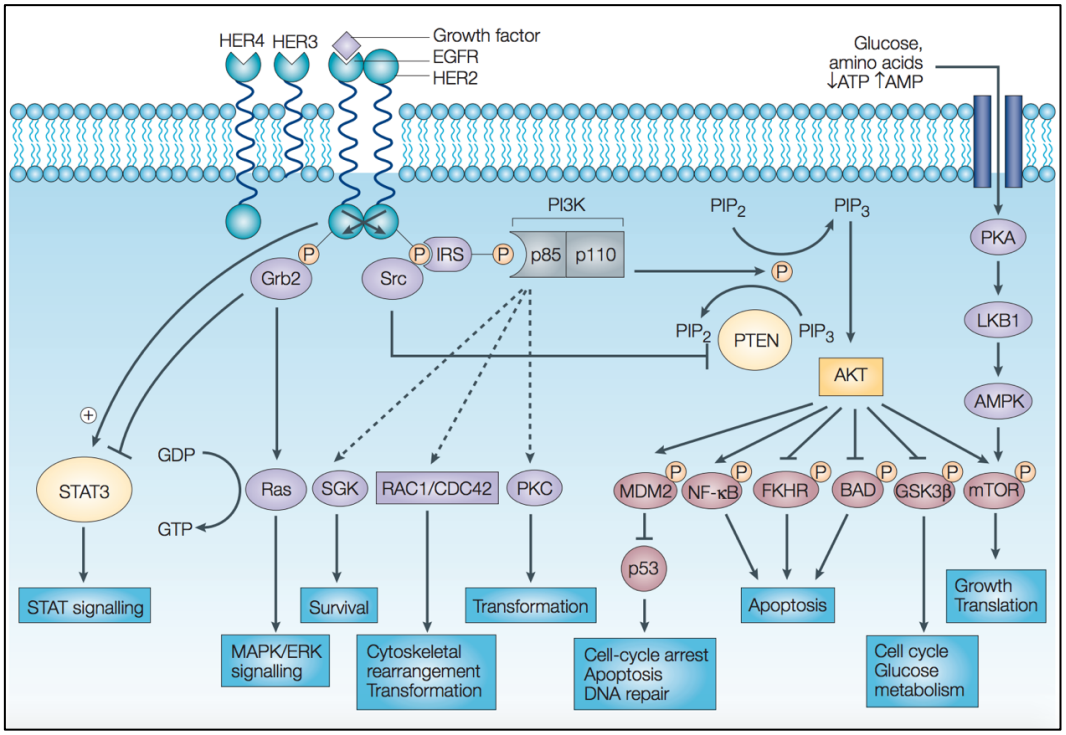

Acquired from: Hennessy BT et al. *Exploiting the PI3K/AKT pathway for cancer drug discovery.* Nat Rev Drug Discov. 2005.

Figure 20: Schematic of Signaling Through the Phosphatidylinositol-3-Kinase (PI3K)/AKT Pathway. The PI3K/AKT and other interrelated pathways are essential in perceiving the effects of external growth signals and associated membrane tyrosine kinases. AKT is activated downstream of PI3K and effects a multitude of targets (9). EGFR, epidermal growth factor receptor; AMPK, AMP-activated protein kinase; mTOR, mammalian target of rapamycin; ERK, extracellular signal regulated kinase; FKHR, forkhead; GDP, guanosine diphosphate; IRS, insulin receptor substrate; GSK3, glycogen synthase kinase 3; MAPK, mitogen-activated protein kinase; NF-κB, nuclear factor-κB, PIP_2, phosphatidylinositol-3,4-diphosphate; PIP_3, phosphatidylinositol-3,4,5-triphosphate; PKC, protein kinase C.

inhibition may therefore not achieve PI3K inhibition, since RUNX1 may negatively regulate PI3K proteins. Rather, RUNX1 activation could work to suppress the hyperactivity of the PI3K pathway commonly seen in BrCa.

Cancer stem cells (CSCs) are another essential area of oncological research today. CSCs are a unique subgroup of the cancer cell population able to propagate new tumors while displaying the ability to self-renew. These traits contribute to the lethal nature of CSCs, as they pose a significant threat when coupled with the canonical hallmarks of cancer (11). CSCs are known to evade current cancer treatment options such as chemotherapy and radiation and are therefore a crucial facilitator in patient relapses and overall aggression of the cancer. By analyzing the downstream gene expression of those genes identified as BrCa drivers in response to RUNX1 depletion and their role in CSC formation and/or maintenance, this project can further examine the tumor suppressor role of RUNX1 in breast cancer and how RUNX1 may work to halt the production of CSCs and the epithelial to mesenchymal transition. With novel insight as to how RUNX1 functions in BrCa, we will be able to develop a safer, more targeted, and more effective plan of action to eradicate one of the deadliest diseases that exists today.

In future studies, the role of RUNX1 in the BCSC population can be analyzed via CD24/CD44 sorting of cells treated with shRUNX1 and shNon-Silencing. The CSC proportions of the culture population can then be found using FACS, as CSCs are characteristically labeled as $CD24^{-}/CD44^{+}$ with regard to cell-surface markers. RNA and protein expression profiles of the predicted BrCa driver genes presented here may be carried out on the RUNX1 depleted BCSC subpopulation. This, in addition to the qPCR data presented here, will develop a clearer picture

of how RUNX1 functions in BrCa progression and aggression. Further studies will also require optimization of inducible CRISPRi, a system designed to deplete RUNX1 upon the addition of the antibiotic doxycycline through the activation of dCas9. Clonal selection and dCas9 expression upon dox-induction has been carried out, though more optimization is needed to yield a knockout greater than 80% at both promoters of RUNX1. This inducible system will provide a real-time snapshot of the effects of RUNX1 depletion, as it can be turned on and off with the use of doxycycline.

Acknowledgements

This research was made possible by funding provided by a summer undergraduate research fellowship (SURF) from the UVM Office of Undergraduate Research and was supported by NIH grant NCI P01 CA082834 (G.S.S., J.L.S.).

A special thank you to my thesis committee and all members of the Stein/Lian lab, especially Janet Stein, Andrew Fritz and Deli Hong, for their support, mentorship and guidance throughout this ongoing project.

Works Cited

1. Nik-Zainal S, Davies H, Staaf J, Ramakrishna M, Glodzik D, Zou X, Martincorena I, Alexandrov LB, Martin S, Wedge DC, Van Loo P, Ju YS, Smid M, Brinkman AB, Morganella S, Aure MR, Lingjaerde OC, Langerod A, Ringner M, Ahn SM, Boyault S, Brock JE, Broeks A, Butler A, Desmedt C, Dirix L, Dronov S, Fatima A, Foekens JA, Gerstung M, Hooijer GK, Jang SJ, Jones DR, Kim HY, King TA, Krishnamurthy S, Lee HJ, Lee JY, Li Y, McLaren S, Menzies A, Mustonen V, O'Meara S, Pauporte I, Pivot X, Purdie CA, Raine K, Ramakrishnan K, Rodriguez-Gonzalez FG, Romieu G, Sieuwerts AM, Simpson PT, Shepherd R, Stebbings L, Stefansson OA, Teague J, Tommasi S, Treilleux I, Van den Eynden GG, Vermeulen P, Vincent-Salomon A, Yates L, Caldas C, van't Veer L, Tutt A, Knappskog S, Tan BK, Jonkers J, Borg A, Ueno NT, Sotiriou C, Viari A, Futreal PA, Campbell PJ, Span PN, Van Laere S, Lakhani SR, Eyfjord JE, Thompson AM, Birney E, Stunnenberg HG, van de Vijver MJ, Martens JW, Borresen-Dale AL, Richardson AL, Kong G, Thomas G, Stratton MR. Landscape of somatic mutations in 560 breast cancer whole-genome sequences. Nature. 2016;534(7605):47-54. Epub 2016/05/03. doi: 10.1038/nature17676. PubMed PMID: 27135926; PMCID: PMC4910866.
2. Banerji S, Cibulskis K, Rangel-Escareno C, Brown KK, Carter SL, Frederick AM, Lawrence MS, Sivachenko AY, Sougnez C, Zou L, Cortes ML, Fernandez-Lopez JC, Peng S, Ardlie KG, Auclair D, Bautista-Pina V, Duke F, Francis J, Jung J, Maffuz-Aziz A, Onofrio RC, Parkin M, Pho NH, Quintanar-Jurado V, Ramos AH, Rebollar-Vega R, Rodriguez-Cuevas S, Romero-Cordoba SL, Schumacher SE, Stransky N, Thompson KM, Uribe-Figueroa L, Baselga J, Beroukhim R, Polyak K, Sgroi DC, Richardson AL, Jimenez-Sanchez G, Lander ES, Gabriel SB, Garraway LA, Golub TR, Melendez-Zajgla J, Toker A, Getz G, Hidalgo-Miranda A, Meyerson M. Sequence analysis of mutations and translocations across breast cancer subtypes. Nature. 2012;486(7403):405-9. Epub 2012/06/23. doi: 10.1038/nature11154. PubMed PMID: 22722202; PMCID: PMC4148686.
3. Hong D, Messier TL, Tye CE, Dobson JR, Fritz AJ, Sikora KR, Browne G, Stein JL, Lian JB, Stein GS. Runx1 stabilizes the mammary epithelial cell phenotype and prevents epithelial to mesenchymal transition. Oncotarget. 2017;8(11):17610-27. Epub 2017/04/15. doi: 10.18632/oncotarget.15381. PubMed PMID: 28407681; PMCID: PMC5392273.
4. Ito Y, Bae SC, Chuang LS. The RUNX family: developmental regulators in cancer. Nat Rev Cancer. 2015;15(2):81-95. Epub 2015/01/17. doi: 10.1038/nrc3877. PubMed PMID: 25592647.
5. Hanahan D, Weinberg RA. Hallmarks of cancer: the next generation. Cell. 2011;144(5):646-74. Epub 2011/03/08. doi: 10.1016/j.cell.2011.02.013. PubMed PMID: 21376230.
6. Kalluri R, Weinberg RA. The basics of epithelial-mesenchymal transition. J Clin Invest. 2009;119(6):1420-8. Epub 2009/06/03. doi: 10.1172/JCI39104. PubMed PMID: 19487818; PMCID: PMC2689101.
7. Paddison PJ, Caudy AA, Bernstein E, Hannon GJ, Conklin DS. Short hairpin RNAs (shRNAs) induce sequence-specific silencing in mammalian cells. Genes Dev. 2002;16(8):948-58. Epub 2002/04/18. doi: 10.1101/gad.981002. PubMed PMID: 11959843; PMCID: PMC152352.
8. Chuang LS, Ito K, Ito Y. RUNX family: Regulation and diversification of roles through interacting proteins. Int J Cancer. 2013;132(6):1260-71. Epub 2012/11/28. doi: 10.1002/ijc.27964. PubMed PMID: 23180629.

9. Hennessy BT, Smith DL, Ram PT, Lu Y, Mills GB. Exploiting the PI3K/AKT pathway for cancer drug discovery. Nat Rev Drug Discov. 2005;4(12):988-1004. Epub 2005/12/13. doi: 10.1038/nrd1902. PubMed PMID: 16341064.
10. Chimge NO, Frenkel B. The RUNX family in breast cancer: relationships with estrogen signaling. Oncogene. 2013;32(17):2121-30. Epub 2012/10/10. doi: 10.1038/onc.2012.328. PubMed PMID: 23045283; PMCID: PMC5770236.
11. Nguyen LV, Vanner R, Dirks P, Eaves CJ. Cancer stem cells: an evolving concept. Nat Rev Cancer. 2012;12(2):133-43. Epub 2012/01/13. doi: 10.1038/nrc3184. PubMed PMID: 22237392.
12. Bill R, Christofori G. The relevance of EMT in breast cancer metastasis: Correlation or causality? FEBS Lett. 2015;589(14):1577-87. Epub 2015/05/17. doi: 10.1016/j.febslet.2015.05.002. PubMed PMID: 25979173.
13. Miller J, Horner A, Stacy T, Lowrey C, Lian JB, Stein G, Nuckolls GH, Speck NA. The core-binding factor beta subunit is required for bone formation and hematopoietic maturation. Nat Genet. 2002;32(4):645-9. Epub 2002/11/16. doi: 10.1038/ng1049. PubMed PMID: 12434155.
14. Taniuchi I, Littman DR. Epigenetic gene silencing by Runx proteins. Oncogene. 2004;23(24):4341-5. Epub 2004/05/25. doi: 10.1038/sj.onc.1207671. PubMed PMID: 15156191.
15. Young DW, Hassan MQ, Pratap J, Galindo M, Zaidi SK, Lee SH, Yang X, Xie R, Javed A, Underwood JM, Furcinitti P, Imbalzano AN, Penman S, Nickerson JA, Montecino MA, Lian JB, Stein JL, van Wijnen AJ, Stein GS. Mitotic occupancy and lineage-specific transcriptional control of rRNA genes by Runx2. Nature. 2007;445(7126):442-6. Epub 2007/01/26. doi: 10.1038/nature05473. PubMed PMID: 17251981.
16. Ramaswamy S, Ross KN, Lander ES, Golub TR. A molecular signature of metastasis in primary solid tumors. Nat Genet. 2003;33(1):49-54. Epub 2002/12/07. doi: 10.1038/ng1060. PubMed PMID: 12469122.
17. Kadota M, Yang HH, Gomez B, Sato M, Clifford RJ, Meerzaman D, Dunn BK, Wakefield LM, Lee MP. Delineating genetic alterations for tumor progression in the MCF10A series of breast cancer cell lines. PLoS One. 2010;5(2):e9201. Epub 2010/02/20. doi: 10.1371/journal.pone.0009201. PubMed PMID: 20169162; PMCID: PMC2821407.
18. Ferrari N, Riggio AI, Mason S, McDonald L, King A, Higgins T, Rosewell I, Neil JC, Smalley MJ, Sansom OJ, Morris J, Cameron ER, Blyth K. Runx2 contributes to the regenerative potential of the mammary epithelium. Sci Rep. 2015;5:15658. Epub 2015/10/23. doi: 10.1038/srep15658. PubMed PMID: 26489514; PMCID: PMC4614940.
19. Ferrari N, McDonald L, Morris JS, Cameron ER, Blyth K. RUNX2 in mammary gland development and breast cancer. J Cell Physiol. 2013;228(6):1137-42. Epub 2012/11/22. doi: 10.1002/jcp.24285. PubMed PMID: 23169547.
20. Kendrick H, Regan JL, Magnay FA, Grigoriadis A, Mitsopoulos C, Zvelebil M, Smalley MJ. Transcriptome analysis of mammary epithelial subpopulations identifies novel determinants of lineage commitment and cell fate. BMC Genomics. 2008;9:591. Epub 2008/12/10. doi: 10.1186/1471-2164-9-591. PubMed PMID: 19063729; PMCID: PMC2629782.
21. Owens TW, Rogers RL, Best S, Ledger A, Mooney AM, Ferguson A, Shore P, Swarbrick A, Ormandy CJ, Simpson PT, Carroll JS, Visvader J, Naylor MJ. Runx2 is a novel regulator of mammary epithelial cell fate in development and breast cancer. Cancer Res. 2014;74(18):5277-86. Epub 2014/07/25. doi: 10.1158/0008-5472.CAN-14-0053. PubMed PMID: 25056120; PMCID: PMC4178131.

22. van Bragt MP, Hu X, Xie Y, Li Z. RUNX1, a transcription factor mutated in breast cancer, controls the fate of ER-positive mammary luminal cells. Elife. 2014;3:e03881. Epub 2014/11/22. doi: 10.7554/eLife.03881. PubMed PMID: 25415051; PMCID: PMC4381933.
23. Sokol ES, Sanduja S, Jin DX, Miller DH, Mathis RA, Gupta PB. Perturbation-expression analysis identifies RUNX1 as a regulator of human mammary stem cell differentiation. PLoS Comput Biol. 2015;11(4):e1004161. Epub 2015/04/22. doi: 10.1371/journal.pcbi.1004161. PubMed PMID: 25894653; PMCID: PMC4404314.
24. Inman CK, Shore P. The osteoblast transcription factor Runx2 is expressed in mammary epithelial cells and mediates osteopontin expression. J Biol Chem. 2003;278(49):48684-9. Epub 2003/09/25. doi: 10.1074/jbc.M308001200. PubMed PMID: 14506237.
25. Inman CK, Li N, Shore P. Oct-1 counteracts autoinhibition of Runx2 DNA binding to form a novel Runx2/Oct-1 complex on the promoter of the mammary gland-specific gene beta-casein. Mol Cell Biol. 2005;25(8):3182-93. Epub 2005/03/31. doi: 10.1128/MCB.25.8.3182-3193.2005. PubMed PMID: 15798204; PMCID: PMC1069618.
26. Ellis MJ, Ding L, Shen D, Luo J, Suman VJ, Wallis JW, Van Tine BA, Hoog J, Goiffon RJ, Goldstein TC, Ng S, Lin L, Crowder R, Snider J, Ballman K, Weber J, Chen K, Koboldt DC, Kandoth C, Schierding WS, McMichael JF, Miller CA, Lu C, Harris CC, McLellan MD, Wendl MC, DeSchryver K, Allred DC, Esserman L, Unzeitig G, Margenthaler J, Babiera GV, Marcom PK, Guenther JM, Leitch M, Hunt K, Olson J, Tao Y, Maher CA, Fulton LL, Fulton RS, Harrison M, Oberkfell B, Du F, Demeter R, Vickery TL, Elhammali A, Piwnica-Worms H, McDonald S, Watson M, Dooling DJ, Ota D, Chang LW, Bose R, Ley TJ, Piwnica-Worms D, Stuart JM, Wilson RK, Mardis ER. Whole-genome analysis informs breast cancer response to aromatase inhibition. Nature. 2012;486(7403):353-60. Epub 2012/06/23. doi: 10.1038/nature11143. PubMed PMID: 22722193; PMCID: PMC3383766.
27. Cancer Genome Atlas N. Comprehensive molecular portraits of human breast tumours. Nature. 2012;490(7418):61-70. Epub 2012/09/25. doi: 10.1038/nature11412. PubMed PMID: 23000897; PMCID: PMC3465532.
28. Cornen S, Guille A, Adelaide J, Addou-Klouche L, Finetti P, Saade MR, Manai M, Carbuccia N, Bekhouche I, Letessier A, Raynaud S, Charafe-Jauffret E, Jacquemier J, Spicuglia S, de The H, Viens P, Bertucci F, Birnbaum D, Chaffanet M. Candidate luminal B breast cancer genes identified by genome, gene expression and DNA methylation profiling. PLoS One. 2014;9(1):e81843. Epub 2014/01/15. doi: 10.1371/journal.pone.0081843. PubMed PMID: 24416132; PMCID: PMC3886975.
29. Wu D, Ozaki T, Yoshihara Y, Kubo N, Nakagawara A. Runt-related transcription factor 1 (RUNX1) stimulates tumor suppressor p53 protein in response to DNA damage through complex formation and acetylation. J Biol Chem. 2013;288(2):1353-64. Epub 2012/11/14. doi: 10.1074/jbc.M112.402594. PubMed PMID: 23148227; PMCID: PMC3543018.
30. Curtis C, Shah SP, Chin SF, Turashvili G, Rueda OM, Dunning MJ, Speed D, Lynch AG, Samarajiwa S, Yuan Y, Graf S, Ha G, Haffari G, Bashashati A, Russell R, McKinney S, Group M, Langerod A, Green A, Provenzano E, Wishart G, Pinder S, Watson P, Markowetz F, Murphy L, Ellis I, Purushotham A, Borresen-Dale AL, Brenton JD, Tavare S, Caldas C, Aparicio S. The genomic and transcriptomic architecture of 2,000 breast tumours reveals novel subgroups. Nature. 2012;486(7403):346-52. Epub 2012/04/24. doi: 10.1038/nature10983. PubMed PMID: 22522925; PMCID: PMC3440846.

31. Liu YN, Lee WW, Wang CY, Chao TH, Chen Y, Chen JH. Regulatory mechanisms controlling human E-cadherin gene expression. Oncogene. 2005;24(56):8277-90. Epub 2005/08/24. doi: 10.1038/sj.onc.1208991. PubMed PMID: 16116478.
32. Pleasance ED, Cheetham RK, Stephens PJ, McBride DJ, Humphray SJ, Greenman CD, Varela I, Lin ML, Ordonez GR, Bignell GR, Ye K, Alipaz J, Bauer MJ, Beare D, Butler A, Carter RJ, Chen L, Cox AJ, Edkins S, Kokko-Gonzales PI, Gormley NA, Grocock RJ, Haudenschild CD, Hims MM, James T, Jia M, Kingsbury Z, Leroy C, Marshall J, Menzies A, Mudie LJ, Ning Z, Royce T, Schulz-Trieglaff OB, Spiridou A, Stebbings LA, Szajkowski L, Teague J, Williamson D, Chin L, Ross MT, Campbell PJ, Bentley DR, Futreal PA, Stratton MR. A comprehensive catalogue of somatic mutations from a human cancer genome. Nature. 2010;463(7278):191-6. Epub 2009/12/18. doi: 10.1038/nature08658. PubMed PMID: 20016485; PMCID: PMC3145108.
33. Stephens PJ, Tarpey PS, Davies H, Van Loo P, Greenman C, Wedge DC, Nik-Zainal S, Martin S, Varela I, Bignell GR, Yates LR, Papaemmanuil E, Beare D, Butler A, Cheverton A, Gamble J, Hinton J, Jia M, Jayakumar A, Jones D, Latimer C, Lau KW, McLaren S, McBride DJ, Menzies A, Mudie L, Raine K, Rad R, Chapman MS, Teague J, Easton D, Langerod A, Oslo Breast Cancer C, Lee MT, Shen CY, Tee BT, Huimin BW, Broeks A, Vargas AC, Turashvili G, Martens J, Fatima A, Miron P, Chin SF, Thomas G, Boyault S, Mariani O, Lakhani SR, van de Vijver M, van 't Veer L, Foekens J, Desmedt C, Sotiriou C, Tutt A, Caldas C, Reis-Filho JS, Aparicio SA, Salomon AV, Borresen-Dale AL, Richardson AL, Campbell PJ, Futreal PA, Stratton MR. The landscape of cancer genes and mutational processes in breast cancer. Nature. 2012;486(7403):400-4. Epub 2012/06/23. doi: 10.1038/nature11017. PubMed PMID: 22722201; PMCID: PMC3428862.
34. Shah SP, Roth A, Goya R, Oloumi A, Ha G, Zhao Y, Turashvili G, Ding J, Tse K, Haffari G, Bashashati A, Prentice LM, Khattra J, Burleigh A, Yap D, Bernard V, McPherson A, Shumansky K, Crisan A, Giuliany R, Heravi-Moussavi A, Rosner J, Lai D, Birol I, Varhol R, Tam A, Dhalla N, Zeng T, Ma K, Chan SK, Griffith M, Moradian A, Cheng SW, Morin GB, Watson P, Gelmon K, Chia S, Chin SF, Curtis C, Rueda OM, Pharoah PD, Damaraju S, Mackey J, Hoon K, Harkins T, Tadigotla V, Sigaroudinia M, Gascard P, Tlsty T, Costello JF, Meyer IM, Eaves CJ, Wasserman WW, Jones S, Huntsman D, Hirst M, Caldas C, Marra MA, Aparicio S. The clonal and mutational evolution spectrum of primary triple-negative breast cancers. Nature. 2012;486(7403):395-9. Epub 2012/04/13. doi: 10.1038/nature10933. PubMed PMID: 22495314; PMCID: PMC3863681.
35. Lawrence MS, Stojanov P, Mermel CH, Robinson JT, Garraway LA, Golub TR, Meyerson M, Gabriel SB, Lander ES, Getz G. Discovery and saturation analysis of cancer genes across 21 tumour types. Nature. 2014;505(7484):495-501. Epub 2014/01/07. doi: 10.1038/nature12912. PubMed PMID: 24390350; PMCID: PMC4048962.
36. Stratton MR, Campbell PJ, Futreal PA. The cancer genome. Nature. 2009;458(7239):719-24. Epub 2009/04/11. doi: 10.1038/nature07943. PubMed PMID: 19360079; PMCID: PMC2821689.
37. van der Oost J, Westra ER, Jackson RN, Wiedenheft B. Unravelling the structural and mechanistic basis of CRISPR-Cas systems. Nat Rev Microbiol. 2014;12(7):479-92. Epub 2014/06/10. doi: 10.1038/nrmicro3279. PubMed PMID: 24909109; PMCID: PMC4225775.
38. Moore CB, Guthrie EH, Huang MT, Taxman DJ. Short hairpin RNA (shRNA): design, delivery, and assessment of gene knockdown. Methods Mol Biol. 2010;629:141-58. Epub 2010/04/14. doi: 10.1007/978-1-60761-657-3_10. PubMed PMID: 20387148; PMCID: PMC3679364.

39. Rao DD, Vorhies JS, Senzer N, Nemunaitis J. siRNA vs. shRNA: similarities and differences. Adv Drug Deliv Rev. 2009;61(9):746-59. Epub 2009/04/25. doi: 10.1016/j.addr.2009.04.004. PubMed PMID: 19389436.
40. Mandegar MA, Huebsch N, Frolov EB, Shin E, Truong A, Olvera MP, Chan AH, Miyaoka Y, Holmes K, Spencer CI, Judge LM, Gordon DE, Eskildsen TV, Villalta JE, Horlbeck MA, Gilbert LA, Krogan NJ, Sheikh SP, Weissman JS, Qi LS, So PL, Conklin BR. CRISPR Interference Efficiently Induces Specific and Reversible Gene Silencing in Human iPSCs. Cell Stem Cell. 2016;18(4):541-53. Epub 2016/03/15. doi: 10.1016/j.stem.2016.01.022. PubMed PMID: 26971820; PMCID: PMC4830697.
41. Larson MH, Gilbert LA, Wang X, Lim WA, Weissman JS, Qi LS. CRISPR interference (CRISPRi) for sequence-specific control of gene expression. Nat Protoc. 2013;8(11):2180-96. Epub 2013/10/19. doi: 10.1038/nprot.2013.132. PubMed PMID: 24136345; PMCID: PMC3922765.
42. Garrett R, Grisham CM. Biochemistry. 5th ed. Belmont, CA: Brooks/Cole, Cengage Learning; 2013. xxxviii, 1169, 48, 22 p. p.
43. Taxman DJ, Livingstone LR, Zhang J, Conti BJ, Iocca HA, Williams KL, Lich JD, Ting JP, Reed W. Criteria for effective design, construction, and gene knockdown by shRNA vectors. BMC Biotechnol. 2006;6:7. Epub 2006/01/26. doi: 10.1186/1472-6750-6-7. PubMed PMID: 16433925; PMCID: PMC1409772.
44. Pushparaj PN, Aarthi JJ, Manikandan J, Kumar SD. siRNA, miRNA, and shRNA: in vivo applications. J Dent Res. 2008;87(11):992-1003. Epub 2008/10/24. doi: 10.1177/154405910808701109. PubMed PMID: 18946005.
45. Mercado-Matos J, Matthew-Onabanjo AN, Shaw LM. RUNX1 and breast cancer. Oncotarget. 2017;8(23):36934-5. Epub 2017/04/30. doi: 10.18632/oncotarget.17249. PubMed PMID: 28455962; PMCID: PMC5514882.
46. Vanhaesebroeck B, Stephens L, Hawkins P. PI3K signalling: the path to discovery and understanding. Nat Rev Mol Cell Biol. 2012;13(3):195-203. Epub 2012/02/24. doi: 10.1038/nrm3290. PubMed PMID: 22358332.
47. Chen L, Yang L, Yao L, Kuang XY, Zuo WJ, Li S, Qiao F, Liu YR, Cao ZG, Zhou SL, Zhou XY, Yang WT, Shi JX, Huang W, Hu X, Shao ZM. Characterization of PIK3CA and PIK3R1 somatic mutations in Chinese breast cancer patients. Nat Commun. 2018;9(1):1357. Epub 2018/04/11. doi: 10.1038/s41467-018-03867-9. PubMed PMID: 29636477; PMCID: PMC5893593.
48. Fruman DA, Rommel C. PI3K and cancer: lessons, challenges and opportunities. Nat Rev Drug Discov. 2014;13(2):140-56. Epub 2014/02/01. doi: 10.1038/nrd4204. PubMed PMID: 24481312; PMCID: PMC3994981.
49. Thorpe LM, Yuzugullu H, Zhao JJ. PI3K in cancer: divergent roles of isoforms, modes of activation and therapeutic targeting. Nat Rev Cancer. 2015;15(1):7-24. Epub 2014/12/24. doi: 10.1038/nrc3860. PubMed PMID: 25533673; PMCID: PMC4384662.